

Abstract

Dixit, Ravindra Krishna. Sliding Mode Observation and Control for Semiactive Vehicle Suspensions. (Under the direction of Dr. Greg Buckner).

This thesis investigates the application of robust, nonlinear observation and control strategies, namely sliding mode observation and control (SMOC), to semiactive vehicle suspensions using a model reference approach. The vehicle suspension models include realistic nonlinearities in the spring and magnetorheological (MR) damper elements, and the nonlinear reference models incorporate skyhook damping. Since full state measurement is difficult to achieve in practice, a sliding mode observer (SMO) that requires only suspension deflection as a measured input is developed. The performance and robustness of sliding mode control (SMC), SMO, and SMOC is demonstrated through comprehensive computer simulations and compared to popular alternatives. The results of these simulations reveal the benefits of sliding mode observation and control for improved ride quality, and should be directly transferable to commercial semiactive vehicle suspension implementations.

Sliding Mode Observation and Control for Semiactive Vehicle Suspensions

By
Ravindra Dixit

A Thesis submitted to the Graduate Faculty of
North Carolina State University
in partial fulfillment of the
requirements for the degree of
Master of Science

Department of Mechanical and Aerospace Engineering

Raleigh
November 2001

APPROVED BY:

CHAIR OF ADVISORY COMMITTEE

Dedication

I dedicate this thesis
to my Parents
Leela and Krishna Dixit

Biography

Ravindra Dixit was born on February 7, 1976 in Pune, India. He graduated with a Bachelor of Engineering degree in Mechanical Engineering from Maharashtra Institute of Technology in Pune, India, in June 1997. After graduation he pursued a job at *TELCO* (Tata Engineering and Locomotive Co. Ltd., Pune), which is the largest manufacturer of commercial vehicles in India. In the first six months of his training he joined the R & D Department and was involved in the design and testing of braking systems. In the next six months he was posted to the Production Engineering Dept. where he managed a front axle assembly line. After the training period he joined the QAPM (Quality Assurance and Process Management Dept.) of the Tata Indica Minicar project. This was the first car to be manufactured indigenously in India. As a quality and process management engineer he was responsible for the door and underbody assembly lines and interacted with management and shop personnel at all levels.

He then went on to pursue graduate study in the Mechanical Engineering Department of the University of Toledo, OH for a semester, where he specialized in Finite Element Analysis and Experimental Methods.

He then went on to the master's program at North Carolina State University working under the direction of Professor Gregory D. Buckner. His primary research focused on control algorithms for semiactive suspensions. As a part of his research he also assisted Dr. Buckner in manufacturing a quarter car suspension test rig. He aspires to pursue his career in the controls engineering industry.

Acknowledgements

First I would like to thank Dr. Greg Buckner for being my advisor and mentor. He was extremely supportive in all ways and working with him for one and a half years was an enriching experience.

I would also like to thank my committee members for extending their support. I extend my thanks to Dr. Ro for broadening my knowledge of MIMO control systems; Dr. Silverberg for being very supportive and friendly during my stay at MMRC and Dr. Grant for extending his support from the ECE Dept.

I take this opportunity to thank the Mechanical Engineering Department and its staff for their wonderful support. A special thanks to Mike and Skip in the workshop for all their help and cooperation.

I would also like to thank all my friends at NC State for making my stay in Raleigh a memorable one.

Last but not least, I would like to thank my parents; my brother Ashwin and my sister Vidya for all their support.

Table of Contents

List of Tables	vi
List of Figures	vii
1 Introduction	1
2 System Models	4
2.1 Quarter Car Model	4
2.2 Linear State Equations	5
2.3 Nonlinear Equations of Motion	5
2.4 MR Damper Dynamics	7
3 Controller Development	10
3.1 Model Reference Control	11
3.1.1 Skyhook Reference Models	11
3.2 Sliding Mode Control Law	13
3.2.1 Equivalent Control Law	14
3.2.2 Discontinuous performance term	15
3.3 Sliding Mode Observation	16
3.3.1 SMO Design	16
4 Simulations	20
4.1 Vehicle and Road Parameters	21
4.2 Controller Parameters	22
4.3 Simulation Set I: Linear vs. Nonlinear Skyhook Reference Models	23
4.4 Simulation Set II: Fixed-Gain vs. Variable-Gain SMC	26
4.5 Simulation Set III: Variable-Gain SMC vs. LQR	29
4.6 Simulation Set IV: Sliding Mode Observation and Control (SMOC)	32
4.7 Simulation Set V: SMOC with Parametric Uncertainties	36
4.8 Simulation Set VI: SMC with Unmeasurable Road Inputs	39
5 Conclusions	43
List of References	45

List of Tables

4.1	Simulation summary	20
4.2	Nonlinear vehicle suspension parameters	21
4.3	Road input parameters	22
4.4	Linear vehicle suspension parameters	30
4.5	Performance comparison: SMC vs. LQR for nonlinear system	32

List of Figures

2.1	Semiactive quarter-vehicle suspension model	4
2.2	Stiction model	6
2.3	Block diagram of semiactive suspension control system	7
2.4	Steady-state damping characteristics of a composite MR damper	8
3.1	Model reference control structure	11
3.2	Fourth-order skyhook reference model	12
3.3	Second-order skyhook reference model	13
3.4	Structure of a nonlinear Luenberger observer	17
3.5	Sliding mode observer structure	19
4.1	Preliminary simulations to compare performance of linear and nonlinear reference models	24
4.2	Reference model responses to sinusoidal terrain inputs - comparison to baseline SMC	24
4.3	Reference model responses to sinusoidal terrain inputs - comparison to baseline SMC	26
4.4	Fixed-gain SMC and nonlinear skyhook reference model responses to white noise terrain input (k=10)	27
4.5	Variable-gain SMC and nonlinear skyhook reference model responses to white noise terrain input)	28
4.6	Variable switching gain $k(t)$ and control current $i(t)$ - white noise terrain input) . . .	28
4.7	FFT magnitude plot of control current $i(t)$)	29
4.8	Comparison of LQR and SMC responses using linear state equations - bump terrain input	31
4.9	Comparison of LQR and SMC responses using nonlinear state equations - bump terrain input	32
4.10	Comparison of LQR and SMC control for a nonlinear suspension and sine wave road input	33
4.11	Comparison of actual, Luenburger, and SMO responses - sinusoidal terrain input . .	34
4.12	SMOC for a bump road input	35
4.13	SMOC for a sine wave road input	36
4.14	Comparison of actual and SMO responses with parametric uncertainties - sinusoidal terrain input	37
4.15	Comparison of actual and SMO responses with parametric uncertainties - white noise terrain input	37
4.16	Comparison of skyhook reference and SMOC responses with parametric uncertainties - sinusoidal terrain input	38

4.17 Comparison of skyhook reference and SMOC responses with parametric uncertainties - white noise terrain input	38
4.18 Comparison of fourth-order and second-order skyhook reference models - sinusoidal terrain input	40
4.19 Comparison of fourth-order and second-order skyhook reference models - impulse input	40
4.20 SMOC with second-order reference model for sine wave road input	41
4.21 SMOC with second-order reference model for "bump" input	41

Chapter 1

Introduction

Active vehicle suspension systems were introduced in the early 1970's to overcome the drawbacks of passive suspensions, namely the inherent tradeoff between ride quality and handling performance [1,2,3]. Active suspensions use actuators, sensors, and control algorithms to introduce bi-directional control forces to the suspension system. Published research spanning 30 years has demonstrated significant improvements in ride quality and handling performance using prototype active suspensions [4,5,6,7,8]. Actuators for these suspensions are commonly based on hydraulic servo systems [6,9,10,11,12]. Others incorporate sophisticated valving into gas shocks. Crolla et. al. [7] used gas over oil springs and a pendulum mass damper controller for active suspension control. Recent advances in power electronics and brushless motors have enabled electromechanical technologies. Buckner et. al. [4,5] implemented high-bandwidth electromechanical actuators for off-road military vehicles.

Despite the published benefits and recent advances in active suspensions, these systems remain complex, bulky, and expensive and are not common options on production vehicles. Additionally, they typically require considerable power and impose heavy loads on the engine. A notable exception is electromechanical actuator technologies, which allow regeneration of energy otherwise dissipated as heat [4]. Additional design and control challenges inherent in active suspension systems have not fully been resolved. These include actuator nonlinearities, stiction, bandwidth limitations, durability and maintenance issues. The application of active suspensions systems has thus been limited to prototype off-road, military, and racing vehicles.

Semiactive suspensions overcome many of these limitations of active suspensions, although generally with a reduction in achievable ride quality and handling performance [1,2], though some researchers

have concluded that this reduction is quite small [13]. Semiactive suspensions can be considerably more cost effective, compact, and functionally simple as they require only a variable damper and a few sensors to achieve adequate performance. Conventional semiactive suspensions rely on servo-controlled damper valves to achieve “continuously variable damping” [2,15,16,17]. The primary drawbacks of such systems are associated with a large number of mechanical parts. These systems suffer many of the bandwidth, durability, and maintenance limitations of active suspensions. Hence even semiactive systems have not gained commercial popularity.

The recent advent of commercial magnetorheological (MR) fluid dampers has made it possible to vary the damping force almost instantaneously with very few mechanical parts [14,18]. This reduction in complexity permits high-bandwidth, low-power performance with reduced concerns about durability and maintenance. These semiactive dampers contain MR fluids, which are suspensions of micron-sized, magnetizable particles in an oil-based fluid. In the absence of magnetic fields, these fluids exhibit Newtonian behavior. The application of an external magnetic field causes the particles to become aligned with the field, and dramatically changes the effective viscosity of the fluid. MR dampers are controlled by manipulating a low-power coil current to vary the effective damping coefficient [14,18]. Recently, Carerra has introduced MagneShocksTM for semiactive vehicle suspensions [14] and Delphi Automotive Systems has introduced MagnerideTM, both using MR fluid technology to enable damping adjustments at frequencies up to 1000 Hz. This bandwidth is 10 times faster than conventional servo valve dampers [18], and has rejuvenated research into semiactive suspension systems.

The performance of semiactive suspension systems relies heavily on real-time control strategies. Early research on semiactive control strategies focused primarily on linear techniques, such as optimal control [16,19-21] and skyhook control [17,22-24]. However, vehicle suspensions contain dynamic nonlinearities associated with springs and dampers [4], sliding friction in joints [4,25], and suspension kinematics [26] which significantly affect ride quality and handling performance. Vehicle suspensions are also subjected to parameter variations, like changes in damping and stiffness over extended time periods, that adversely affect time-invariant and non-robust control strategies.

More recently, semiactive control research has focused more on nonlinear control techniques. Gordon and Best [27] extended previous nonlinear optimal designs to semiactive systems and incorporated dynamic parameter optimization. Hedrick and Sohn [17] linearized the vehicle dynamics about an equilibrium point and applied skyhook control to control a semiactive MacPherson strut suspension. Henry and Zeid [28] derived a sub-optimal nonlinear control law, but did not consider spring and

damper nonlinearities. Considerable research effort has concentrated on fuzzy logic, neural networks, and artificial intelligence techniques [15,29,30,31]. The primary advantages of these systems is that complete knowledge of the model dynamics may not be required, and hence nonlinearities may be incorporated easily. Ursu et al. [29] employed artificial intelligence techniques for semiactive suspension design. Cheok et. al. [30] used neural networks and Heuristic Optimal Control (HOC) to derive a self-improving semiactive suspension system. Nicolas, et al. [15], implemented fuzzy logic control with continuously variable damping. Cheok and Huang [31] developed training algorithms for neural models using Lyapunov stability theory and MRAC (Model Reference Adaptive Control). The primary drawbacks of such methods lie in the ad-hoc nature of their tuning and the inability to address robustness factors.

Sliding Mode Control (SMC) is a highly effective nonlinear and robust control strategy. It is insensitive to unmodeled dynamics and parametric uncertainties and has been used effectively in fields like robotics, aerospace, and automotive systems [32]. Kim and Ro [33] developed SMC for a nonlinear active suspension system and compared it to a self-tuning controller. Results showed that SMC significantly improved robust tracking performance when vehicle parameters changed. Alleyne and Hedrick [34] used SMC for a nonlinear actuator in an active vehicle suspension system. Hedrick et. al. [35] demonstrated the effectiveness of SMC for MR semiactive suspension systems using a model following approach.

This thesis investigates the application of robust, nonlinear observation and control strategies, namely sliding mode observation and control (SMOC), to semiactive vehicle suspensions using a model reference approach. The vehicle suspension model includes realistic nonlinearities in the spring and MR damper elements, and the reference models are nonlinear versions of skyhook damping model. Since full state measurement is difficult to achieve in practice, a sliding mode observer (SMO) that requires only suspension deflection as a measured input is developed. The performance and robustness of sliding mode control (SMC), SMO, and SMOC is demonstrated through comprehensive computer simulations and compared to popular alternatives.

Chapter 2

System Models

2.1 Quarter Car Model

Quarter-vehicle models are used routinely in the analysis and design of vehicle suspension systems [1,2,16,17,21]. Typically, the state equations are linear and the model parameters are time-invariant, and such assumptions yield reasonable results for many applications [16,19,20]. In reality, however, quarter-vehicle dynamics contain nonlinearities associated with kinematics, bump-stops, stiction and hardening springs that can be significant in the design of active and semiactive suspensions [25-28]. Figure 2.1 shows the basic structure of a semiactive quarter car model.

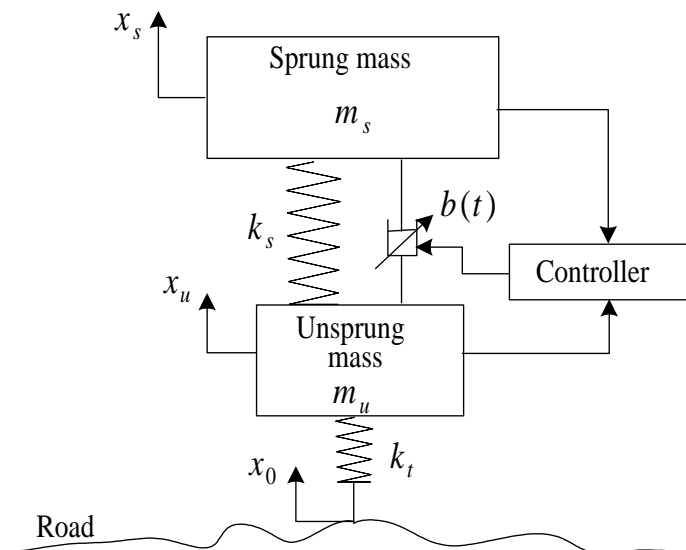


Figure 2.1: Semiactive quarter-vehicle suspension model

In this model, x_s and x_u represent the sprung and unsprung mass absolute displacements, respectively and x_0 represents a road disturbance. k_s and k_t represent suspension and tire stiffness, both typically linear with respect to suspension deflection. In typical passive models, damping is assumed to be viscous with a constant damping coefficient. For semiactive systems, however, the damping coefficient is the manipulated variable of the control system, and is thus time varying $b(t)$.

2.2 Linear State Equations

Linear state equations for the semiactive, quarter-vehicle model can be derived using a straightforward Newtonian approach:

$$\begin{aligned} m_s \ddot{x}_s &= -k_s(x_s - x_u) - b(t)(\dot{x}_s - \dot{x}_u) \\ m_u \ddot{x}_u &= k_s(x_s - x_u) + b(t)(\dot{x}_s - \dot{x}_u) - k_t(x_u - x_0) \end{aligned} \quad (2.1)$$

where $b(t)$ is a constant for passive suspensions but is bounded by physical damper constraints in semiactive suspensions $b_0 \leq b(t) \leq b_{\max}$ [19,35].

2.3 Nonlinear Equations of Motion

Nonlinear effects, like those related to stiction, bump stops, and hardening springs can be readily accommodated by replacing linear constitutive relations with appropriate nonlinear relations. For example, stiction is a “hard” damping nonlinearity associated with vehicle suspensions that can be incorporated by modifying the viscous damping term. Stiction is caused by dry friction between the piston and cylinder, and occurs whenever the relative velocity between the sliding surfaces is zero and the static friction coefficient is significantly greater than the dynamic friction coefficient. Numerous models have been developed to represent stiction [38,39]. The model used in this research is shown in Figure 2.2.

This model incorporates the static friction force D_s (defined only when the suspension’s relative velocity is zero) and the dynamic friction force C_s (for all other velocities):

$$f_{st} = \begin{cases} f_a & v = 0, |f_a| < D_s \\ D_s \operatorname{sgn}(f_a) & v = 0, |f_a| \geq D_s \\ C_s \operatorname{sgn}(v) + b_0 v & \text{otherwise} \end{cases} \quad (2.2)$$

2.4 MR Damper Dynamics

Magneto-rheological (MR) fluids are suspensions of micron-sized, magnetizable particles in an oil-based fluid. In the absence of magnetic fields, these fluids exhibit Newtonian behavior. The application of an external magnetic field causes the particles to become aligned with the field, and dramatically changes the effective viscosity of the fluid. Depending on the strength of this applied magnetic field, the viscosity (or yield strength) of MR fluids can reach that of Bingham solids, making them well-suited to semiactive damping applications [40].

Semiactive vehicle suspensions are controlled by manipulating the coil current in the MR damper to vary its effective damping coefficient. This approach is represented in the block diagram of Figure 2.3.

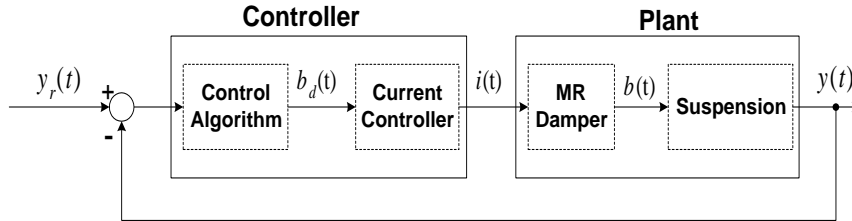


Figure 2.3: Block diagram of semiactive suspension control system

The desired damping coefficient $b_d(t)$ determined by the suspension control algorithm must be converted to a coil control current. This current depends on the nonlinear force-velocity characteristics of the MR damper, which vary significantly among manufacturers and models. The force-velocity relationships used in this research are based on a generic composite of high performance MR dampers used for vibration isolation and automotive semiactive suspensions [24,41]. The composite steady-state damping characteristics are represented in Figure 2.4. Note that the stiction characteristics described earlier (Section 2.3), are lumped into this composite MR damper model.

As this figure shows, the composite MR damper exhibits bilinear force-velocity characteristics. The steady-state damping coefficient $b_{ss}(t)$ is bounded and proportional to the applied current $i(t)$:

$$\begin{aligned} b_0 \leq b_{ss}(t) \leq b_{\max} \text{ for } 0 \leq i(t) \leq i_{\max} \text{ and} \\ b_{ss}(t) = b_0 + \mu i(t) \end{aligned} \quad (2.5)$$

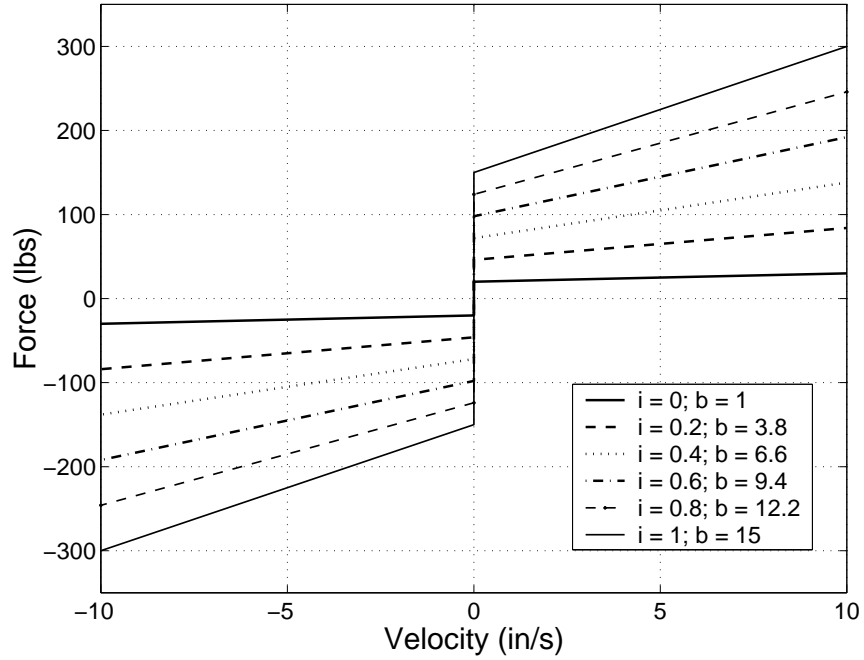


Figure 2.4: Steady-state damping characteristics of a composite MR damper

Here μ is a constant that linearly scales the damping resulting from the applied coil current $i(t)$. The steady-state current required to achieve the desired damping coefficient $b_d(t)$ is thus:

$$i(t) = \frac{b_d(t) - b_0}{\mu} \quad (2.6)$$

Although the response times of commercial MR fluids are relatively fast, phase lag is associated with the inductance of the control coils. The dynamic response of a typical MR shock absorber can be modeled as first-order, linear, with a rise time of τ (typically 1-10 ms [18,24,40]):

$$b(s) = \frac{b_{ss}}{\tau s + 1} \quad (2.7)$$

This MR damper model assumes that the static friction force D_s is equal to the dynamic friction force C_s (an assumption supported by experimental research [24,41]). Note that C_s is not fixed, but

is time-varying, bounded, and proportional to the applied current:

$$\begin{aligned} C_{s \min} &\leq C_s(t) \leq C_{s \max} \\ C_s(t) &= C_{s \min} + \psi i(t) \end{aligned} \tag{2.8}$$

Chapter 3

Controller Development

High-performance control of semiactive vehicle suspensions is complicated by nonlinearities and uncertainties in the system dynamics and by the need for accurate state information. For these reasons, practical implementations require nonlinear controllers and observers that are robust to uncertainties and disturbances.

In this section, a robust sliding mode controller is developed for the nonlinear, semiactive vehicle suspension system (2.4). Ideally, this controller will be robust to parameter variations (so-called structured uncertainties) and unmodeled dynamics (unstructured uncertainties). The controller is developed using a model reference approach that emulates the performance of the well-known sky-hook damping model [22,24,33,35].

Advanced control strategies like model reference sliding mode control require knowledge of the absolute sprung mass velocity and displacement, states that are not readily measurable. This fact is frequently overlooked in simulations, but cannot be ignored in vehicle implementations. In this research, a robust state observer is developed to provide state estimation using only measured suspension deflection as an input.

The development of each controller component is described in the following sections.

3.1 Model Reference Control

Model reference control (MRC) is a strategy based on specifying the desired closed-loop performance through the selection of a stable reference model. Figure 3.1 shows the block diagram of a typical

MRC structure.

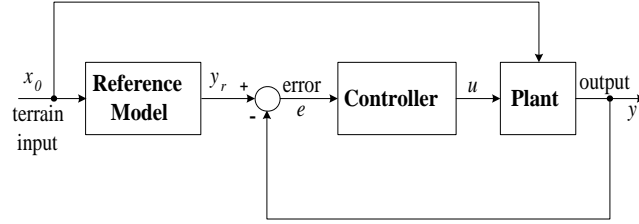


Figure 3.1: Model reference control structure

The plant output y is made to track the reference model output y_r using feedback control u . Although the MRC structure of Figure 3.1 is straightforward and intuitive, there are limitations to its implementation. For example, reference model selection may be severely limited by physical plant constraints [24,35], and realization of the reference model dynamics typically requires that the plant be minimum phase [48]. In addition, MRC may require accurate knowledge of states and inputs that are not measurable [33,45].

3.1.1 Skyhook Reference Models

An excellent reference model for semiactive vehicle suspension control can be derived from Karnopp's skyhook damping strategy [17,22-24]. An inertially grounded damper (the “skyhook” damper, b_{sky}) provides damping proportional to the absolute velocity of the sprung mass. A fourth-order realization of this reference model (which assumes road inputs are known) is shown in Figure 3.2.

The skyhook reference model can be linear or nonlinear, depending on whether the spring and damping elements (k_s and b_s) are linear or nonlinear. The linear state equations for the fourth-order skyhook reference model are:

$$\begin{aligned} m_s \ddot{x}_{sr} &= -k_s (x_{sr} - x_{ur}) - b_s (\dot{x}_{sr} - \dot{x}_{ur}) - b_{sky} \dot{x}_{sr} \\ m_u \ddot{x}_{ur} &= k_s (x_{sr} - x_{ur}) + b_s (\dot{x}_{sr} - \dot{x}_{ur}) - k_t (x_{ur} - x_0) \end{aligned} \quad (3.1)$$

The nonlinear, fourth-order skyhook reference state equations are:

$$\begin{aligned} m_s \ddot{x}_{sr} &= -f_s - b_s (\dot{x}_{sr} - \dot{x}_{ur}) - b_{sky} \dot{x}_{sr} \\ m_u \ddot{x}_{ur} &= f_s + b_s (\dot{x}_{sr} - \dot{x}_{ur}) - k_t (x_{ur} - x_0) \end{aligned} \quad (3.2)$$

Here f_{st} and f_a are the nonlinear stiction and hardening spring relations defined in (2.2) and (2.3).

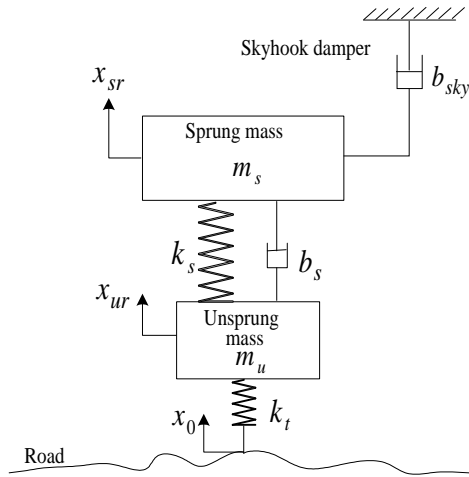


Figure 3.2: Fourth-order skyhook reference model

These fourth-order skyhook reference models are widely used in the design and analysis of vehicle suspension systems, particularly the linear version (3.1). However, these models require knowledge of terrain input x_0 , which is generally very difficult to measure on a moving vehicle. A more realistic skyhook model would assume that the terrain inputs are not known, and consider the unsprung mass position as a system input. This is generally a good approximation given that the tire stiffness is much higher than the suspension spring stiffness. The resulting skyhook reference model is second-order, as shown in Figure 3.3.

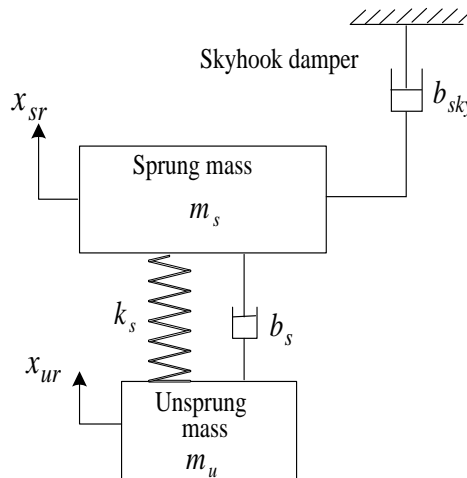


Figure 3.3: Second-order skyhook reference model

The nonlinear, second-order skyhook reference model state equations are:

$$m_s \ddot{x}_{sr} = -f_s - b_s (\dot{x}_{sr} - \dot{x}_{ur}) - b_{sky} \dot{x}_{sr} \quad (3.3)$$

Recent advances in electronics have made it possible to scan the terrain ahead of moving vehicles, enabling control algorithms that assume knowledge of the terrain, even preview control [16,19]. For this reason, both skyhook reference models (the fourth-order model, which assumes knowledge of terrain inputs and the second-order model, which assumes this information is not available) have been utilized in this research.

3.2 Sliding Mode Control Law

Sliding Mode Control (SMC) is a high-performance, robust control strategy for uncertain nonlinear systems. The control law consists of two components: a stabilizing equivalent control law u_{eq} and a performance term u_p . Model reference SMC is based upon the formulation of a “sliding surface” of tracking errors, such that perfect tracking is equivalent to remaining on this surface for all time. The performance term is discontinuous over the sliding surface, and governs the reachability and global asymptotic stability of the system. The reference tracking errors \mathbf{e} and sliding surface $s(\mathbf{e}, t)$ are defined:

$$\begin{aligned} \mathbf{e} &= \left[(x_r - x) \quad (\dot{x}_r - \dot{x}) \quad \cdots \quad \left(\frac{d^{n-1}x_r}{dt^{n-1}} - \frac{d^{n-1}x}{dt^{n-1}} \right) \right] \\ s(\mathbf{e}, t) &= \dot{\mathbf{e}} + \lambda \mathbf{e} \end{aligned} \quad (3.4)$$

where λ is a positive design scalar and $x_r(t)$ and $x(t)$ represent the states of the reference model and the plant, respectively. A system remaining on such a sliding surface is said to be in “sliding mode” and has zero tracking error, as the unique solution to $s(\mathbf{e}, t) = 0$ is $\mathbf{e}(t) = 0$ [46]. This reduces a high-order tracking problem to a first-order regulator problem in s .

For the specific case of tracking a skyhook reference model, the sliding surface can be defined:

$$\begin{aligned} \mathbf{e} &= [x_{sr}(t) - x_s(t)] \\ s(\mathbf{e}, t) &= \dot{\mathbf{e}} + \lambda \mathbf{e} \end{aligned} \quad (3.5)$$

where $x_{sr}(t)$ is the sprung mass vertical displacement of the skyhook reference model.

Constructing a control strategy so that the system is in sliding motion is accomplished by formulating a continuous feedback control law u_{eq} and adding to it a discontinuous performance term u_p :

$$u = u_{eq} + u_p \quad (3.6)$$

3.2.1 Equivalent Control Law

The equivalent control law is derived from the nonlinear state equations (2.4) and the defined sliding surface (3.5). Neglecting the MR damper dynamics (2.7), the quarter-vehicle dynamics can be expressed:

$$\begin{aligned} \ddot{x}_s &= -\frac{f_s + f_{st}}{m_s} - \frac{b_0}{m_s} (\dot{x}_s - \dot{x}_u) - \frac{1}{m_s} (\dot{x}_s - \dot{x}_u) b(t) \\ &= f(x) + g(x)u \end{aligned} \quad (3.7)$$

where $u = b(t)$ is the desired damping coefficient determined by the controller, and:

$$\begin{aligned} f(x) &= -\frac{f_s + f_{st}}{m_s} - \frac{b_0}{m_s} (\dot{x}_s - \dot{x}_u) \\ g(x) &= -\frac{1}{m_s} (\dot{x}_s - \dot{x}_u) \end{aligned} \quad (3.8)$$

Since $f(x)$ and $g(x)$ are not known precisely (due to parametric uncertainties and unmodeled dynamics), SMC must assume that modeling uncertainties are bounded. The additive plant uncertainties can be bounded by a constant (or known function) $F = F(x, \dot{x})$ [46]:

$$\left| f(x) - \hat{f}(x) \right| \leq F \quad (3.9)$$

where $\hat{f}(x)$ and $\hat{g}(x)$ are uncertain models of $f(x)$ and $g(x)$. The multiplicative plant uncertainties can be bounded by known functions (or constants) $g_{\min} = g_{\min}(x, \dot{x})$ and $g_{\max} = g_{\max}(x, \dot{x})$ [46]:

$$0 \leq g_{\min} \leq \hat{g}(x) \leq g_{\max} \quad (3.10)$$

As shown in [46], it is advantageous to choose $\hat{g}(x)$ as the geometric mean of g_{\min} and g_{\max} :

$$\hat{g}(x) = \sqrt{g_{\min} g_{\max}} \quad (3.11)$$

The equivalent control law is designed to maintain the system on the sliding surface in the absence of modeling uncertainties. If $f(x)$ and $g(x)$ were known perfectly, equivalent control would be enough to keep the system (15) on the sliding surface for all time ($s = 0 \Rightarrow \dot{s} = 0 \quad \forall t$). With modeling uncertainties, however, the sliding condition can be determined by combining (3.5) and (3.7):

$$\begin{aligned}
\dot{s}(\mathbf{e}, t) &= \ddot{\mathbf{e}} + \lambda \dot{\mathbf{e}} \\
&= \ddot{x}_{sr} - \ddot{x}_s + \lambda \dot{\mathbf{e}} \\
&= \ddot{x}_{sr} - \left(\hat{f}(x) + \hat{g}(x) u \right) + \lambda \dot{\mathbf{e}}
\end{aligned} \tag{3.12}$$

The equivalent control law is thus:

$$u_{eq} = \hat{g}(x)^{-1} \left(-\hat{f}(x) + \ddot{x}_{sr} + \lambda \dot{\mathbf{e}} \right) \tag{3.13}$$

3.2.2 Discontinuous performance term

Uncertainties in $f(x)$ and $g(x)$ may cause the system to leave sliding surface defined by (3.5). To ensure robustness, a discontinuous performance term u_p (also known as a switching term) is introduced. When the system leaves the sliding surface (i.e. $s \neq 0$), this term drives the system states back onto the sliding surface by making it attractive:

$$u_p = -\hat{g}(x)^{-1} k \cdot \text{sgn}(s) \tag{3.14}$$

where sgn is the signum function defined by:

$$\begin{aligned}
\text{sgn}(s) &= +1 \text{ if } s > 0 \\
\text{sgn}(s) &= -1 \text{ if } s < 0
\end{aligned} \tag{3.15}$$

The switching gain k is generally a constant determined by the uncertainty bounds (3.9), but it may be time- or state-dependent. In this research, the switching gain is state-dependent, which allows for reduced control effort in areas where modeling uncertainties are small. The condition on k for robust stability is:

$$k \geq \alpha(F + \eta) + (\alpha - 1) |\hat{g}(x) \cdot u_{eq}| \tag{3.16}$$

where $\alpha = \sqrt{g_{\max}/g_{\min}}$, F is defined in (3.9), and η is a strictly positive constant defined using the η -reachability condition [32,46]:

$$\frac{1}{2} \frac{d}{dt} s^2 \leq -\eta |s| \tag{3.17}$$

It can be shown [46] that with this choice of switching gain, global asymptotic stability is ensured. Combining (3.6), (3.13), and (3.14) the SMC law is:

$$u = u_{eq} + u_p = \hat{g}(x)^{-1} \left[\left(-\hat{f}(x) + \ddot{x}_{sr} + \lambda \dot{e} \right) - k \operatorname{sgn}(s) \right] \quad (3.18)$$

3.3 Sliding Mode Observation

The SMC law (3.18) derived above requires accurate knowledge of the absolute sprung mass displacement and velocity, since these variables are used to formulate the sliding surface. These measurements are not readily attainable on a moving vehicle, however, hence for this research a robust Sliding Mode Observer (SMO) was developed.

3.3.1 SMO Design

Sliding mode observers enable robust, accurate estimation of system states for nonlinear, uncertain systems where conventional observers or Kalman filters perform poorly [8,28]. This section describes the design of a sliding mode observer, which is based on a standard Luenberger observer but includes a discontinuous performance term for robustness.

For state estimation, the nonlinear state equations (2.4) can be expressed in the following form:

$$\begin{aligned} \dot{x} &= Ax + Bv(x, t) + Gx_0 + Df(x, t) \\ y &= Cx \end{aligned} \quad (3.19)$$

where $x = \begin{bmatrix} x_u & \dot{x}_u & x_s & \dot{x}_s \end{bmatrix}^T$ represents the state vector, $v(x, t) = b(t)(\dot{x}_u - \dot{x}_s)$ represents the controlled damping force, $f(x, t) = f_s + f_{st}$ represents suspension nonlinearities, x_0 represents exogenous road inputs, and y represents the measured output (suspension deflection).

A and B are the system and input matrices, respectively. G and D scale the exogenous road inputs and nonlinear system terms, respectively. C is the output matrix.

The block diagram in Figure 3.4 shows the structure of a conventional Luenberger observer, in this case applied to the nonlinear state equations (2.4). The actual plant output y is compared with the observed output, \hat{y} , and the error is used to update the observed states by means of the observer

matrix L . For this general nonlinear application, the separation principle [48] cannot be applied, thus closed loop stability cannot be guaranteed.

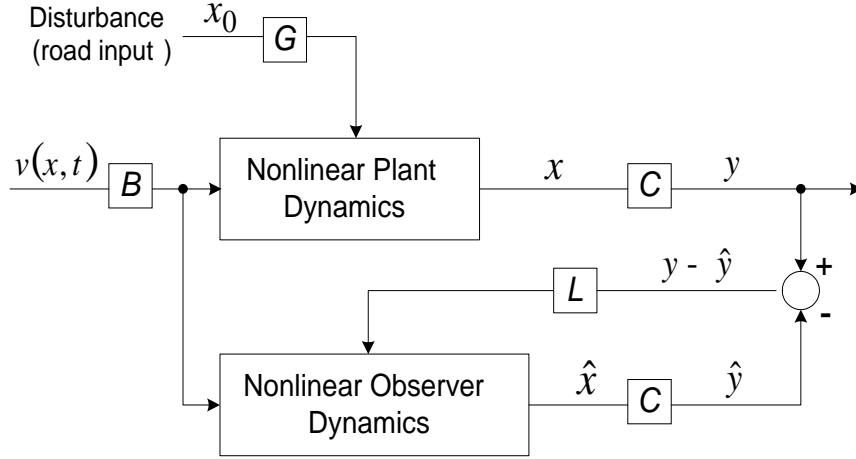


Figure 3.4: Structure of a nonlinear Luenberger observer

Given a nominal model of this plant, the nonlinear observer is represented by [42,43]:

$$\dot{\hat{x}} = A\hat{x} + Bv(\hat{x}, t) + Df(\hat{x}, t) + L(y - \hat{y}) \quad (3.20)$$

where:

\hat{x} represents the estimated state vector

L is the Luenberger observer matrix

The L matrix can be designed [28] by placing the poles of the system matrix $[A-LC]$ to achieve stable error dynamics (3.21).

$$\begin{aligned} e_o &= y - \hat{y} \\ \dot{e}_o &= (A - LC)e_o + Df(e_o, t) + Gx_0 \end{aligned} \quad (3.21)$$

This traditional observer structure cannot guarantee global asymptotic stability, robustness, or convergence in the presence of plant nonlinearities, parametric variations, and disturbances. For this reason, a discontinuous performance term, similar to the SMC term in (3.14), is added for robustness:

$$\dot{\hat{x}} = A\hat{x} + Bv(\hat{x}, t) + Df(\hat{x}, t) + L(y - \hat{y}) + K_0 \text{sgn}(y - \hat{y}) \quad (3.22)$$

where K_0 is the SMO switching gain matrix.

Typically K_0 is designed using LQ techniques [42,44] or Nyquist criteria approaches [28,44]. In this research, the “circle criterion” approach has been used, resulting in the selection of $K_0 = \rho G, \rho \geq 0$ [28]. To avoid chattering, the performance term $K_0 \text{sgn}(y - \hat{y})$ can be constrained to be continuous as long as the system states lie within a boundary layer defined by error limits between the measured and estimated output states:

$$x_p = K_o \cdot \text{sat} \left[\frac{y - \hat{y}}{\phi} \right] \quad (3.23)$$

where ϕ is the boundary layer width. When the observer error exceeds this boundary layer width, the performance term becomes discontinuous. The saturation term is thus defined to be:

$$\text{sat} \left[\frac{y - \hat{y}}{\phi} \right] = \begin{cases} \frac{y - \hat{y}}{\phi} & \text{for } |y - \hat{y}| \leq \phi \\ \text{sgn}(y - \hat{y}) & \text{for } |y - \hat{y}| > \phi \end{cases} \quad (3.24)$$

Combining (3.20) and (3.23) results in the complete SMO law:

$$\begin{aligned} \dot{\hat{x}} &= A\hat{x} + Bv(\hat{x}, t) + Df(\hat{x}, t) + L(y - \hat{y}) + K_0 \text{sat} \left[\frac{y - \hat{y}}{\phi} \right] \\ \hat{y} &= C\hat{x} \end{aligned} \quad (3.25)$$

The structure of this robust observer is illustrated in Figure 3.5.

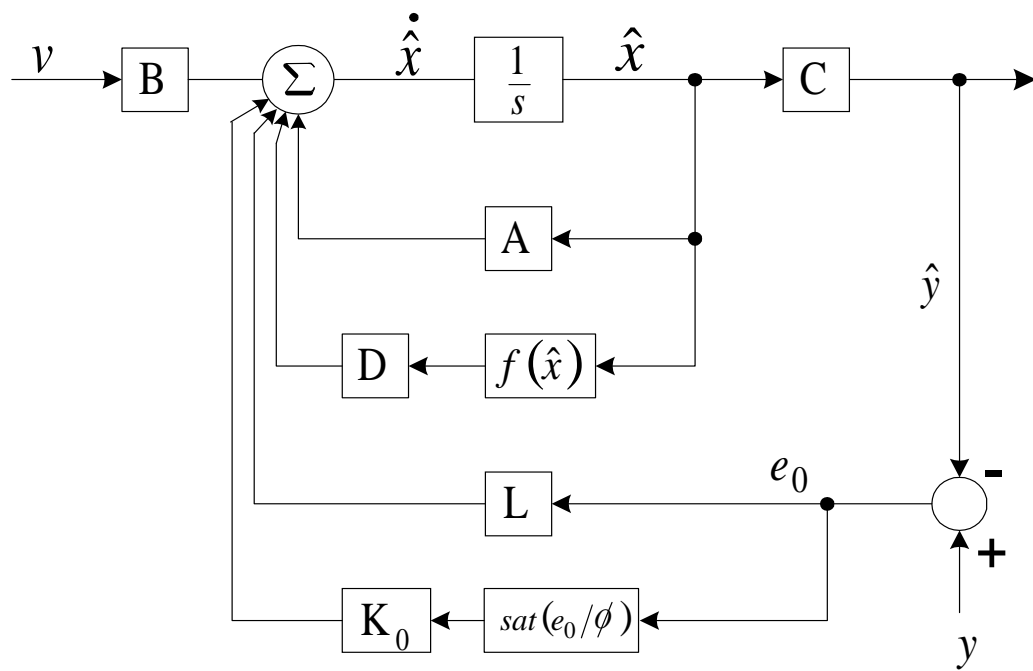


Figure 3.5: Sliding mode observer structure

Chapter 4

Simulations

Extensive computer simulations were conducted to evaluate the effectiveness of sliding mode observation and control for semiactive vehicle suspensions. These simulations utilized vehicle parameters and road input data from other authors to facilitate direct performance comparisons. A comparison with published results using other control algorithms, including LQR and skyhook control, confirmed the performance of the sliding mode algorithms. These simulations are divided into different sets, each with separate objectives, as summarized in Table 4.1.

Table 4.1: Simulation summary

	Simulation Set	Objective
I	Linear vs. Nonlinear Skyhook Reference Models	Study the effects of linear and nonlinear skyhook reference models on baseline SMC performance
II	Fixed-Gain vs. Variable-Gain SMC	Evaluate implications of fixed and variable gain switching on SMC performance
III	Variable-Gain SMC vs. LQR	Compare variable-gain SMC and LQR control laws in the presence of suspension nonlinearities
IV	Sliding Mode Observation and Control (SMOC)	Evaluate the performance of sliding mode observation and control (SMOC)
V	SMOC with Parametric Uncertainties	Investigate the impacts of parametric uncertainties on SMOC
VI	SMOC with Unmeasurable Road Inputs	Compare second-order vs. fourth-order nonlinear skyhook reference models on baseline SMOC

The following sections detail these computer simulation sets.

4.1 Vehicle and Road Parameters

The nonlinear suspension parameters were assumed to be those of a 1992 Hyundai Elantra, as outlined in Ro and Kim [33]. Table 4.2 lists the vehicle suspension parameters used for the nonlinear quarter-vehicle model (2.4) [33].

Table 4.2: Nonlinear vehicle suspension parameters

Parameter	Description	Value
m_s	Sprung mass	240 kg
$k_{s1} = k_1$	Linear suspension stiffness	12394 N/m
k_{s2}	Nonlinear suspension stiffness	-73696 N/m ²
k_{s3}	Nonlinear suspension stiffness	3170400 N/m ³
m_u	Unsprung mass	25 kg
k_t	Tire stiffness	160000 N/m
b_0	Nominal suspension damping	193 Ns/m
$b_p = b_s$	Passive system damping	1385.4 Ns/m
b_{max}	Maximum system damping	2633 Ns/m

Road input data was also taken from the literature to facilitate performance comparisons. Hac et al. used harmonic bumps and waves, filtered white noise, and actual road measurements as road inputs [19,47]. The cosine bumps are described by:

$$x_0(t) = \begin{cases} c(1 - \cos 20\pi(t - 0.3)) & \text{for } t \in [0.3, 0.4] \\ 0 & \text{otherwise} \end{cases} \quad (4.1)$$

where $2c = 0.1$ is the bump height (m). Sinusoidal road inputs are composed of 3 individual sine waves:

$$x_0(t) = 0.1 \sin(3\pi t) + 0.05 \sin(16\pi t) + 0.005 \sin(26\pi t) \quad (4.2)$$

The filtered white noise inputs are the stationary solution of a linear 3^{rd} order filter [47]:

$$\begin{aligned} x_0(t) + (a_1 + a_3) \ddot{x}_0(t) + (a_0 + a_1 a_3) \dot{x}_0(t) + a_0 a_1 x_0(t) \\ = d_1 (\ddot{w}(t) + b_3 \dot{w}(t) + b_0 w(t)) \end{aligned} \quad (4.3)$$

where $w(t)$ is a white noise process with unitary intensity (random seed = 23341) and:

$$a_0^2 = (\alpha_2^2 + \beta^2)v^2 + 4\alpha_2^2\beta^2v^4$$

$$a_1 = \alpha_1 v$$

$$a_2 = 2(\alpha_2^2 - \beta^2)v^2$$

$$a_3 = \sqrt{|(a_2 + 2a_0)|}$$

$$b_0^2 = [\sigma_1^2 \alpha_1 (\alpha_2^2 + \beta^2)^2 + \sigma_2^2 \alpha_1^2 \alpha_2 (\alpha_2^2 + \beta^2)]v^5 / b_4$$

$$b_2 = [2\sigma_1^2 \alpha_1 (\alpha_2^2 - \beta^2) + \sigma_2^2 \alpha_2 (\alpha_1^2 + \alpha_1^2 + \beta^2)]v^3 / b_4$$

$$b_3 = \sqrt{|(b_2 + 2b_0)|}$$

$$b_4 = (\sigma_1^2 \alpha_1 + \sigma_2^2 \alpha_2)v$$

$$d_1 = \sqrt{(b_4/\pi)}$$

The parameters $\alpha_1, \alpha_2, \beta_1, \sigma_1$ and σ_2 depend on the road conditions and are given in Table 4.3.

Table 4.3: Road input parameters

Road Type	$\alpha_1(m^{-1})$	$\alpha_2(m^{-1})$	$\beta_1(m^{-1})$	$\sigma_1(m^2)$	$\sigma_2(m^2)$
Asphalt	0.2	0.05	0.6	7.65×10^{-6}	1.35×10^{-6}
Paved	0.5	0.2	2.0	2.55×10^{-4}	4.5×10^{-3}
Dirt	0.8	0.5	1.1	7.5×10^{-4}	2.5×10^{-4}

4.2 Controller Parameters

The SMC law (3.18) utilizes a controller gain k that can be constant or state dependent. In either case, its magnitude is based on assumed uncertainty bounds between the model and actual vehicle. For these simulations, the additive plant uncertainties $(f(x) - \hat{f}(x))$ were assumed to be bounded within 30%:

$$F = 0.3\hat{f}(x) = 0.3 \left[-\frac{f_s + F_{st}}{m_s} - \frac{b_0}{m_s}(\dot{x}_s - \dot{x}_u) \right] \quad (4.4)$$

Similarly, multiplicative uncertainties associated with \hat{g} were assumed to be bounded within 30%:

$$\begin{aligned} g_{\max} &= -\frac{1}{1.3m_s}(\dot{x}_s - \dot{x}_u) \\ g_{\min} &= -\frac{1}{0.7m_s}(\dot{x}_s - \dot{x}_u) \\ \alpha &= \sqrt{g_{\max}/g_{\min}} \end{aligned} \quad (4.5)$$

SMC design parameters η and λ , defined in (3.12) and (3.17), were tuned for optimal performance over a wide range of terrain inputs:

$$\eta = 1 \quad ; \quad \lambda = 120 \quad (4.6)$$

4.3 Simulation Set I: Linear vs. Nonlinear Skyhook Reference Models

To understand the performance implications of suspension nonlinearities, preliminary simulations were conducted using fourth-order, linear and nonlinear skyhook reference models (3.1) and (3.2), with comparisons to baseline SMC (nonlinear reference model, full-state measurement, road inputs known, fixed switching gain). Figure 4.1 illustrates the structure of these initial simulations.

The nonlinear skyhook reference model incorporated the nonlinear stiffness components (k_{s1} , k_{s2} and k_{s3}) presented in Table 4.2. The linear skyhook reference model contained only the linear stiffness (only the linear spring component k_{s1} of Table 4.2 and damping (only the viscous damper coefficient b_p of Table 4.2 characteristics. For both reference models, setting b_{sky} (the skyhook damping coefficient) to 2000 Ns/m yielded optimum results for the broadest range of road inputs. All simulations were carried out using a 4th-order Runge Kutta solver with a fixed step of 0.001s.

Generally it was observed that for sinusoidal terrain inputs (resulting in large suspension deflections), the ride quality associated with the linear skyhook reference model (in terms of peak-to-peak displacement) was far superior to that of the nonlinear skyhook reference model. Additionally, the “followability” of the linear reference model using baseline SMC was poor, as shown in Figure 4.2. The tracking performance of the nonlinear reference model using the same SMC was significantly better, indicating the significance of system nonlinearities on performance.

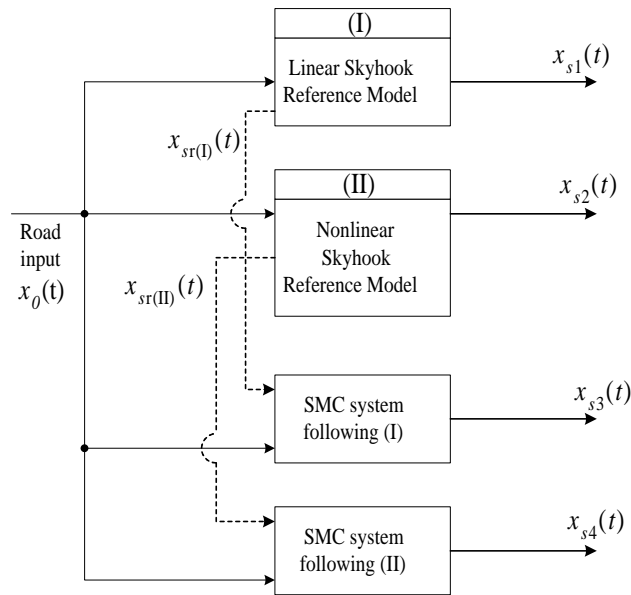


Figure 4.1: Preliminary simulations to compare performance of linear and nonlinear reference models

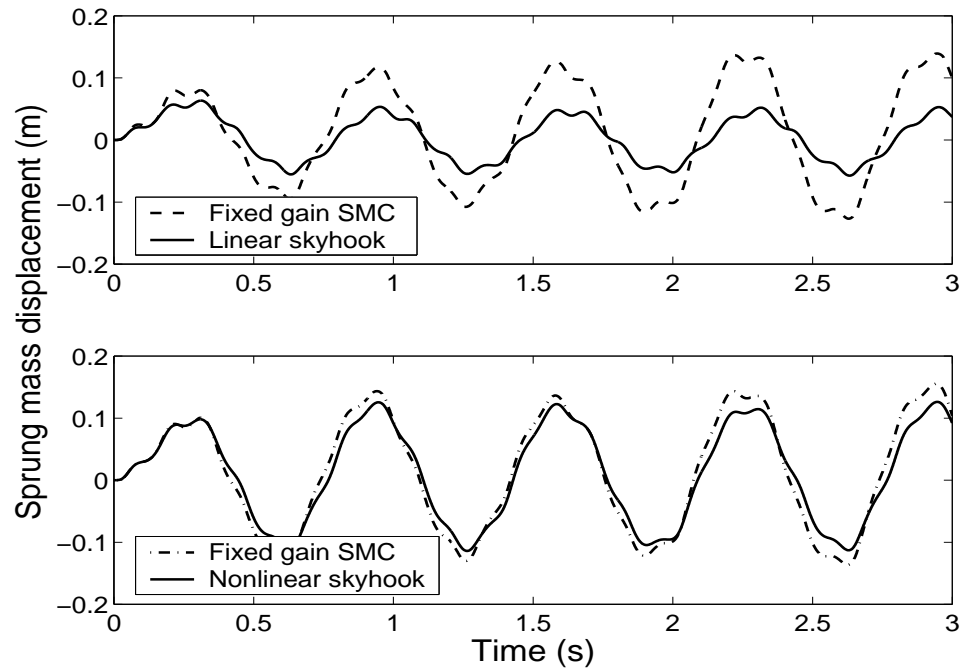


Figure 4.2: Reference model responses to sinusoidal terrain inputs - comparison to baseline SMC

To quantify tracking performance (“followability”), a performance index based on the RMS differences between the appropriate skyhook reference model output and the baseline SMC system output was used:

$$J_1 = \sqrt{\frac{\sum_{i=1}^N (y_{sky_i} - y_{SMC_i})^2}{N}} \times 10^4 \quad (4.7)$$

Additionally, the maximum absolute tracking error between the reference model and the SMC system (in mm) is an indicator of closed-loop performance:

$$J_2 = \max |y_{sky_i} - y_{SMC_i}| \times 10^3 \quad (4.8)$$

For the sinusoidal terrain inputs the performance indices for the nonlinear model were ($J_{1,2} = 196,41$) as compared to ($J_{1,2} = 518,99$) for the linear skyhook model, clearly indicating that the baseline SMC tracked the nonlinear reference model far better than the linear one.

For terrain inputs that resulted in small suspension deflections (i.e. filtered white noise and actual road data) the difference in tracking performance between the linear and nonlinear reference models was negligible. For these cases, the nonlinear reference model and the SMC system were both able to track the linear reference model with reasonable accuracy ($J_{1,2} = 7.2, 2.3$), as illustrated in Figure 4.3.

For intermediate suspension deflections (associated with bumps and step road inputs) the differences in tracking performance were significant, as the baseline SMC algorithm was able to track the nonlinear reference model far better than the linear reference model.

These simulations confirmed that suspension nonlinearities significantly affect the achievable ride quality and tracking performance of semiactive suspensions. Thus the nonlinear skyhook model proved to be a more suitable reference model, since physical followability is an inherent requirement of MRC.

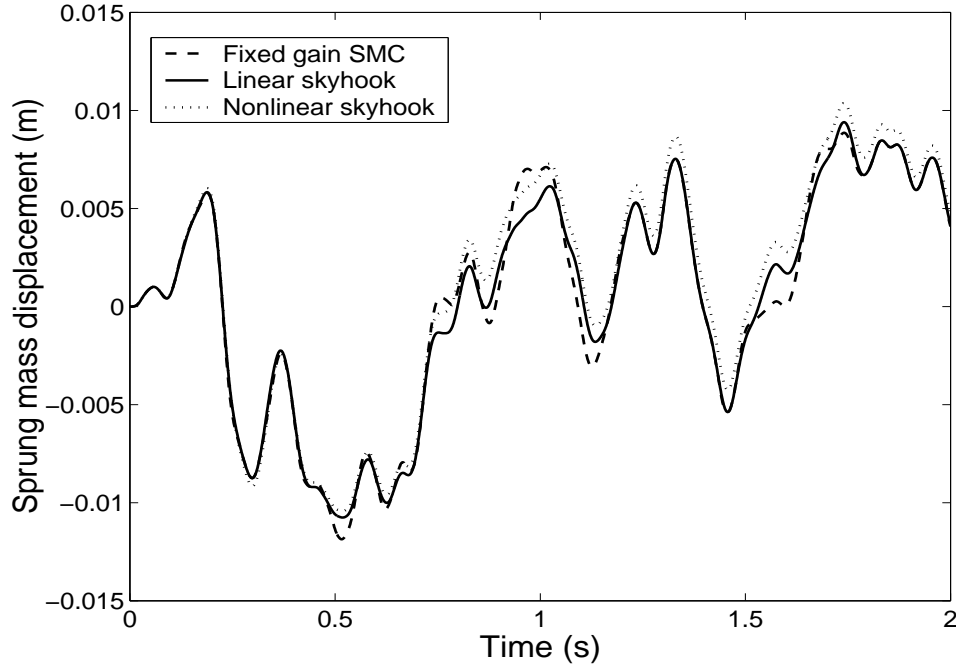


Figure 4.3: Reference model responses to sinusoidal terrain inputs - comparison to baseline SMC

4.4 Simulation Set II: Fixed-Gain vs. Variable-Gain SMC

To understand the performance implications of variable-gain SMC, simulations were conducted using fixed and variable switching gains k in the performance term (3.14). A fixed switching gain of $k = 10$ was selected based on the peak of variable-gain simulations for a variety of road inputs. Results of fixed-gain simulations revealed good tracking performance for road inputs resulting in moderate to large suspension deflections. The performance closely tracked that of the fourth-order, nonlinear skyhook reference model. However, Figure 4.4 shows reduced tracking performance for low amplitude road inputs. For this white noise response, the fixed-gain performance indices were $J_{1,2} = 11.7, 4.3$.

Next, variable-gain SMC was evaluated. The switching gain in (3.14) was assumed to be state dependent as described in (3.16):

$$k \geq \alpha(F + \eta) + (\alpha - 1) |\hat{g}(x) \cdot u_{eq}|$$

Simulations using the same white noise road input clearly indicated that variable-gain switching yielded superior tracking performance. Specifically, the performance cost functions fell to $J_1 = 3.4$

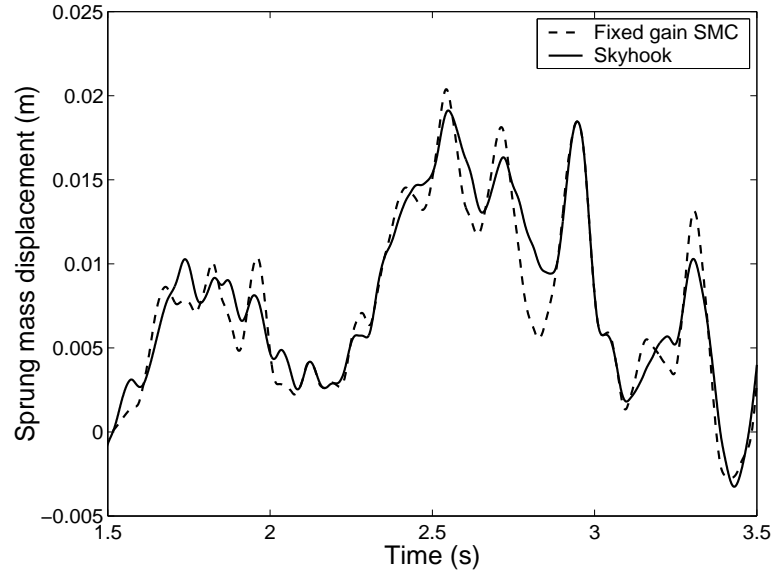


Figure 4.4: Fixed-gain SMC and nonlinear skyhook reference model responses to white noise terrain input ($k=10$)

(from 11.7) and $J_2 = 1.96$ (from 4.3). The performance improvements are clearly illustrated in Figure 4.5.

Figure 4.6 shows how the switching gain $k(t)$ and MR damper current $i(t)$ varied over the course of this simulation.

For this simulation, the average switching gain was $k = 3.51$, and the tracking performance was clearly superior to fixed-gain SMC ($k = 10$). Additionally, the specific power consumption (calculated by integrating current) was $24.6 \text{ mW} / \Omega$ (of MR damper coil resistance) less for variable-gain SMC than for fixed-gain SMC. Similar results were obtained for other road inputs.

Figure (4.7) shows a magnitude spectrum (FFT) of the control current $i(t)$ for this simulation. This figure reveals that the required bandwidth of the MR damper is less than 100 Hz for this terrain input. Note that the MR damper time constant used in these simulations was 1.0 msec, providing more than adequate bandwidth.

Considering the performance indices (4.7) and (4.8), the variable-gain SMC consistently performed better than fixed-gain SMC for low- to moderate-amplitude terrains (resulting in small suspension

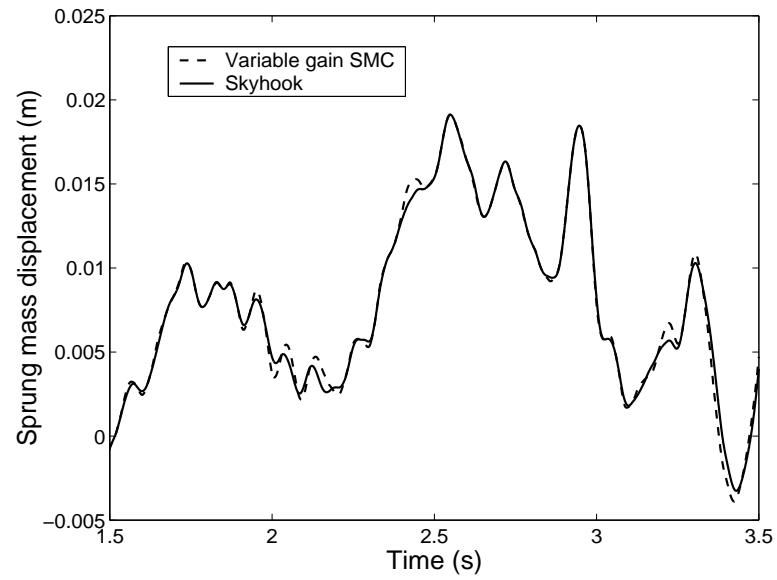


Figure 4.5: Variable-gain SMC and nonlinear skyhook reference model responses to white noise terrain input)

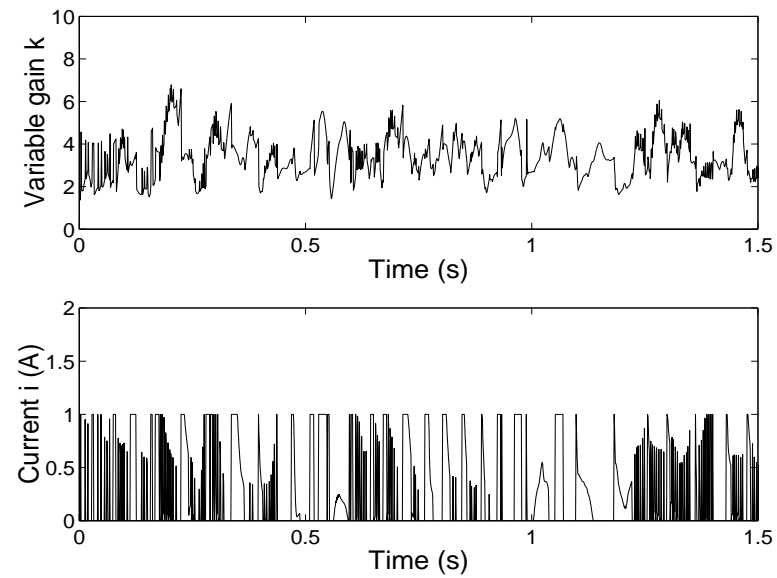


Figure 4.6: Variable switching gain $k(t)$ and control current $i(t)$ - white noise terrain input)

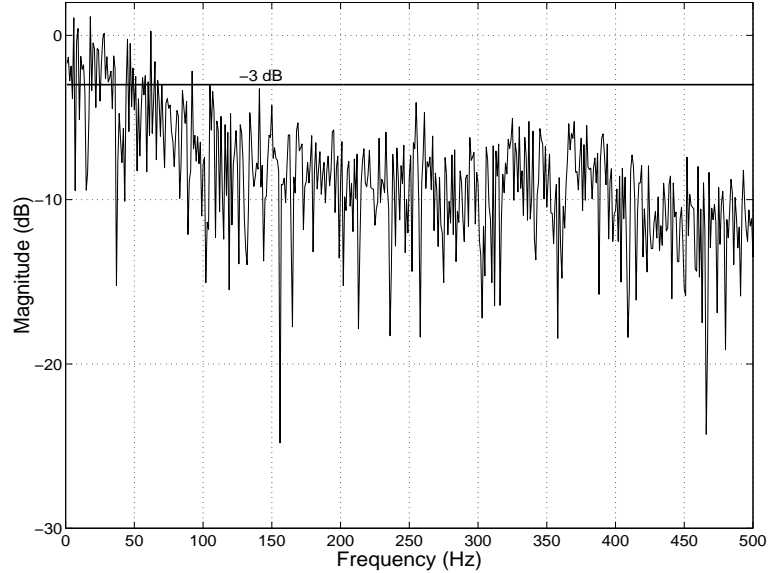


Figure 4.7: FFT magnitude plot of control current $i(t)$

deflections). This improvement is related to the “adaptability” provided by state dependent switching gains. For large-amplitude terrain inputs the differences in performance (between fixed and variable switching gains) were insignificant. Additionally, control activity and actuator bandwidth were reasonable for all simulations.

These simulations clearly revealed the performance advantages of variable-gain SMC, hence this control structure was utilized for all subsequent simulations.

4.5 Simulation Set III: Variable-Gain SMC vs. LQR

LQR synthesis has been widely applied to active and semiactive vehicle suspensions, and has demonstrated excellent performance in linear simulations [2,16,19,45]. To compare the performance of LQR to variable-gain SMC, a series of simulations was conducted using linear and nonlinear vehicle models. The LQR formulation described in [19] is based on the state space plant formulation:

$$\dot{x} = Ax - Bu(\dot{x}_s - \dot{x}_u) + Hw \quad (4.9)$$

where $x = \begin{bmatrix} x_s - x_u & \dot{x}_s & x_u - x_0 & \dot{x}_u \end{bmatrix}^T$ is the state vector, $w = \dot{x}_0$ is the road input, and:

$$A = \begin{bmatrix} 0 & 1 & 0 & -1 \\ -k_s/m_1 & -b_0/m_1 & 0 & b_0/m_1 \\ 0 & 0 & 0 & 1 \\ k_s/m_2 & b_0/m_2 & -k_u/m_2 & -b_0/m_2 \end{bmatrix}$$

$$B = \begin{bmatrix} 0 & 1/m_1 & 0 & -1/m_2 \end{bmatrix}^T$$

$$H = \begin{bmatrix} 0 & 0 & -1/m_2 & 0 \end{bmatrix}^T$$

The LQR synthesis parameters (contained in the Q_1 , Q_n , R , and N matrices defined below) are related to the vehicle parameters defined in Table 4.4:

$$Q_1 = \begin{bmatrix} k_1^2 + \rho_1 m_1^2 & k_1 b_{\min} & 0 & -k b_{\min} \\ k_1 b_{\min} & b_{\min}^2 & 0 & -b_{\min}^2 \\ 0 & 0 & \rho_2 m_1^2 & 0 \\ -k_1 b & -b^2 & 0 & b^2 \end{bmatrix}$$

$$N = \frac{1}{m_1^2} \begin{bmatrix} -k_1 & -b_{\min} & 0 & b_{\min} \end{bmatrix}; \quad R = \frac{1}{m_1^2};$$

$$Q_n = Q_1 - NR^{-1}N^T$$

Table 4.4: Linear vehicle suspension parameters

Parameter	Description	Value
m_1	Sprung mass	290 kg
k_1	Suspension stiffness	10440 N/m
m_2	Unsprung mass	29 kg
k_2	Tire stiffness	104400 N/m
b_{\min}	Minimum system damping	145 Ns/m
b_p	Passive system damping	1392 Ns/m
b_{\max}	Maximum system damping	2784 Ns/m

And the LQR control law is expressed:

$$u = -R^{-1} (N^T + B^T P) x(t) \quad (4.10)$$

where P is a positive definite solution of the Ricatti Equation:

$$PA_n + A_nP - PBR^{-1}B^TP + Q_n = 0 \quad (4.11)$$

To facilitate a direct comparison with published results [19], a “bump” road input was used for these simulations. Full state feedback was assumed for both controllers. Figure 4.8 compares the output responses of LQR and SMC for the linear quarter-vehicle model.

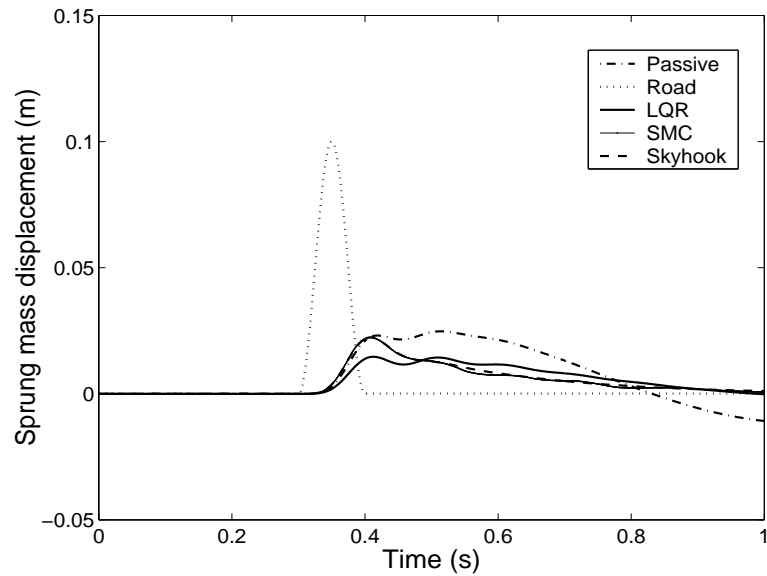


Figure 4.8: Comparison of LQR and SMC responses using linear state equations - bump terrain input

For this linear model, the LQR performance is nearly identical to the fourth-order, linear skyhook reference model, and far superior to the passive response. Similarly, the variable-gain SMC performance tracks the reference model quite well.

As described in Section 2.3, real vehicle suspensions contain nonlinearities that significantly affect the output response. It is important to evaluate the performance implications of these nonlinearities on linear control strategies like LQR. For this reason, simulations were conducted using the nonlinear state equations (2.4) to compare the performance of variable-gain SMC (3.18) and LQR control laws. The nonlinear vehicle parameters used in these simulations are summarized in Table 4.2.

As shown in Figures 4.9 and 4.10, LQR performance degraded substantially (compared to the fourth-order, nonlinear skyhook reference model) with the introduction of dynamic nonlinearities. Table 4.5 quantifies this reduction in performance using the indices of (4.7) and (4.8). Similar results were obtained for a variety of road inputs. Note, however, that the output response of the variable-gain SMC is very similar to the reference model. These simulation results clearly indicate the limitations of linear controls when realistic nonlinearities are considered.

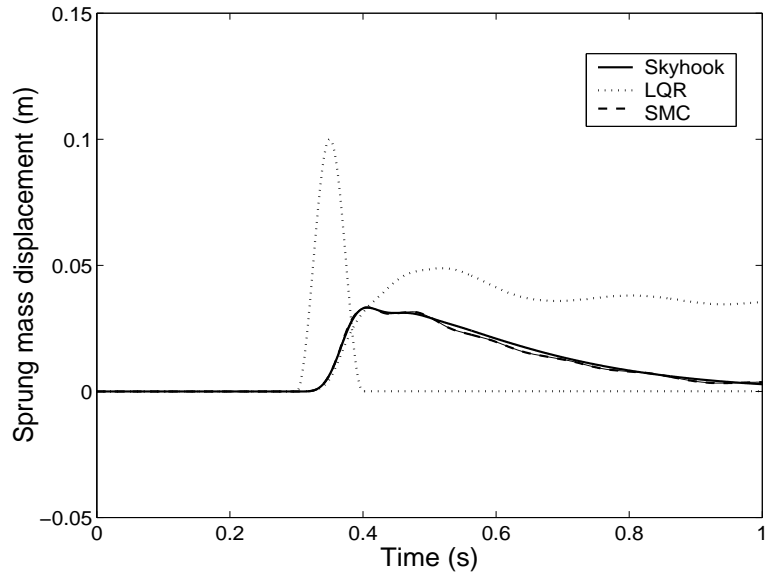


Figure 4.9: Comparison of LQR and SMC responses using nonlinear state equations - bump terrain input

Table 4.5: Performance comparison: SMC vs. LQR for nonlinear system

	Bump input		Sine wave input	
	J_1	J_2	J_1	J_2
SMC	24.3	3.6	91.7	18.8
LQR	268.0	34.6	578.6	99.1

4.6 Simulation Set IV: Sliding Mode Observation and Control (SMOC)

The SMC law (3.18) requires accurate knowledge of the absolute sprung mass displacement and velocity, since these variables are used to formulate the sliding surface. These measurements are not

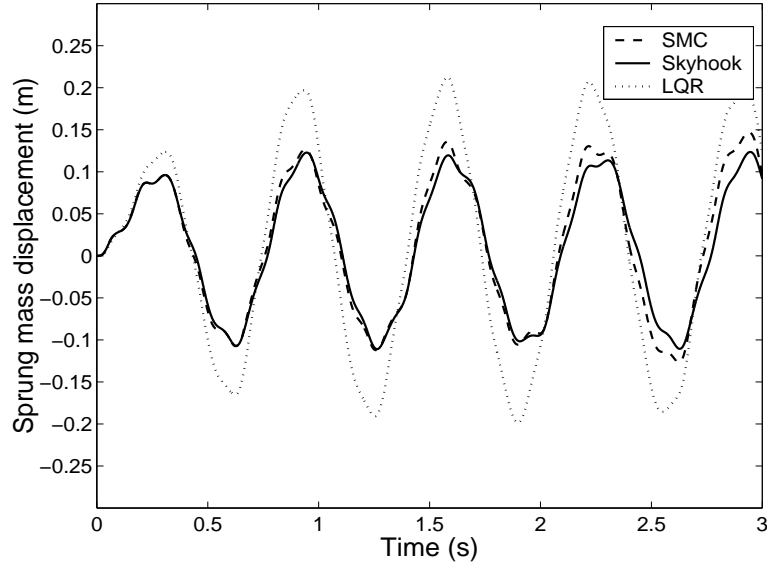


Figure 4.10: Comparison of LQR and SMC control for a nonlinear suspension and sine wave road input

readily attainable on a moving vehicle, however, hence for this research a robust Sliding Mode Observer (SMO) was developed. The structure of this observer, introduced in Section 3.3, is described by equation (3.25):

$$\begin{aligned}\dot{\hat{x}} &= A\hat{x} + Bv(\hat{x}, t) + Df(\hat{x}, t) + L(y - \hat{y}) + K_0 \text{sat} \left[\frac{y - \hat{y}}{\phi} \right] \\ \hat{y} &= C\hat{x}\end{aligned}\tag{4.12}$$

The state matrices of this equation were specified to be consistent with previous simulations:

$$A = \begin{bmatrix} 0 & 1 & 0 & 0 \\ -(k_s + k_t)/m_u & -b_0/m_u & k_t/m_u & b_0/m_u \\ 0 & 0 & 0 & 1 \\ k_s/m_s & b_0/m_s & -k_s/m_s & -b_0/m_s \end{bmatrix}$$

$$B = \begin{bmatrix} 0 & -1/m_u & 0 & 1/m_s \end{bmatrix}^T$$

$$C = \begin{bmatrix} 1 & 0 & -1 & 0 \end{bmatrix}$$

$$D = \begin{bmatrix} 0 & 1/m_u & 0 & -1/m_s \end{bmatrix}$$

$$G = \begin{bmatrix} 0 & k_t/m_u & 0 & 0 \end{bmatrix}^T$$

The observer feedback matrix L was designed to place the tracking error poles (3.21) at $[-23.09 \pm 70.58i, -21.16 \pm 12.27i]$, resulting in $L = [40 \ 40 \ -40 \ -400]^T$. The switching gain matrix and boundary layer width were set to $K_0 = G$, $\phi = 0.001$.

To evaluate the performance of SMO, simulations were conducted using the nonlinear state equations (2.4) and a variety of terrain inputs. Figure 4.6 shows that SMO estimate of sprung mass displacement is nearly indistinguishable from the actual output for a sinusoidal terrain input. For comparison, this figure also shows the output of nonlinear Luenberger observer (without the performance switching term (3.23)), which is clearly inferior. To separate observer performance from controller performance in this simulation, the observed states were not used by the controller (full state measurement was assumed).

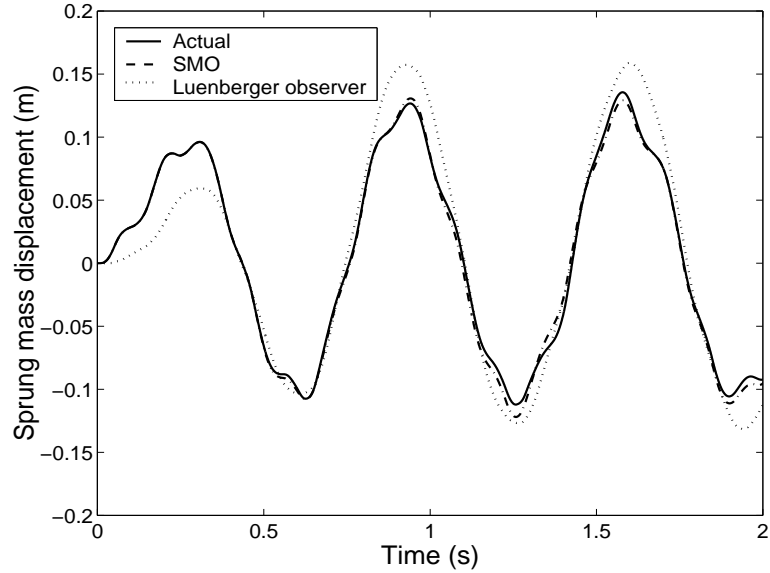


Figure 4.11: Comparison of actual, Luenberger, and SMO responses - sinusoidal terrain input

To quantify observer performance, two additional performance indices were designed based on the RMS and peak errors between actual outputs and observed outputs:

$$J_3 = \sqrt{\frac{\sum_{i=1}^N (y_{plant_i} - y_{SMO_i})^2}{N}} \times 10^4 \quad (4.13)$$

$$J_4 = \max |y_{plant_i} - y_{SMO_i}| \times 10^3 \quad (4.14)$$

These indices reveal that the SMO performance is far superior to the Luenberger observer ($J_{3,4} = 54.6, 11.6$ compared to $J_{3,4} = 314.9, 71.2$) for the nonlinear state equations. Similar results were obtained for a variety of road inputs.

Performance using combined sliding mode observation and control (SMOC, using estimated state information for the control law) was also very good. Figures 4.12 and 4.13 show the performance of SMOC for “bump” and sinusoidal terrain inputs, respectively.

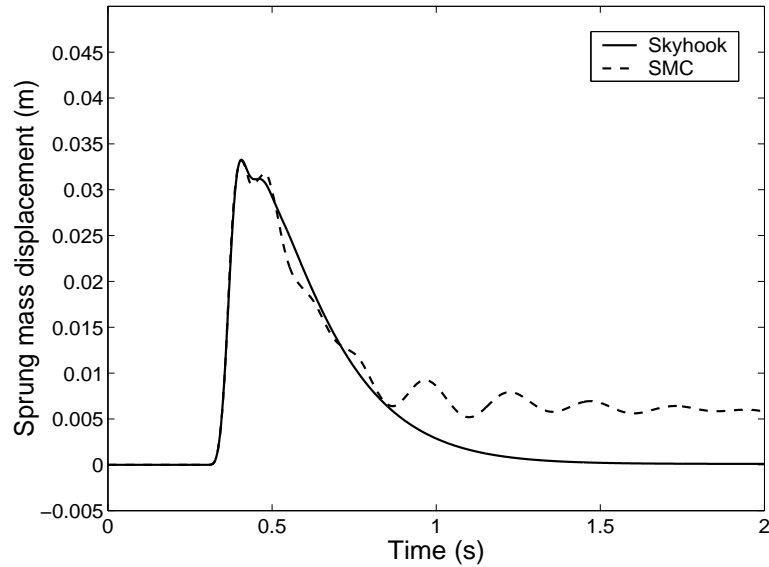


Figure 4.12: SMOC for a bump road input

For sudden road inputs like bumps and steps, SMOC yielded acceptable performance, but errors due to stiction could not be eliminated completely. However, for continuously varying terrain inputs like sinusoids and white noise, SMOC performed accurately, without any significant stiction errors.

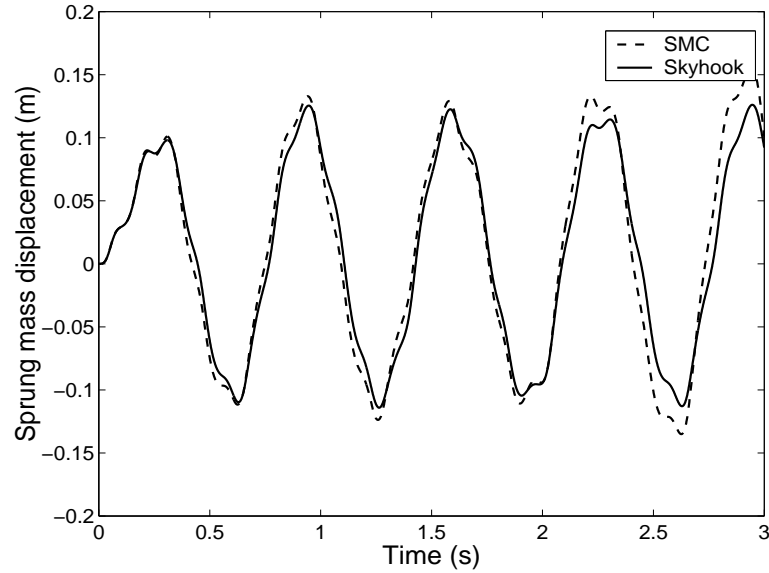


Figure 4.13: SMOC for a sine wave road input

4.7 Simulation Set V: SMOC with Parametric Uncertainties

The preceding SMO and SMOC simulations did not include parametric uncertainties in the state equations. Although the variable switching gains were based on 30% bounds on additive and multiplicative plant uncertainties (3.9) and (3.10), these parameters remained at their nominal values. To investigate the effects of parametric uncertainties on observer performance and controller robustness, simulations were conducted using 10% and 25% variations in spring stiffness (k_{s1}) and sprung mass (m_s), respectively.

Figures 4.14 and 4.15 show the actual and observed sprung mass displacements to sinusoidal and white noise terrain inputs. These simulations clearly show the performance benefits of the observer switching term (3.23), as the estimation error was acceptable, particularly for the white noise road inputs. Generally, it was observed that observer performance was better for rapidly changing road inputs, like the white noise. Similar results were obtained for a variety of terrain inputs.

Simulations were conducted to evaluate the performance implications of parametric uncertainties using combined sliding mode observation and control (SMOC). Figures 4.16 and 4.17 show the performance of SMOC for sinusoidal and white noise terrain inputs, respectively.

The impact of parametric uncertainties can be evaluated by comparing Figure 4.16 to Figure 4.13

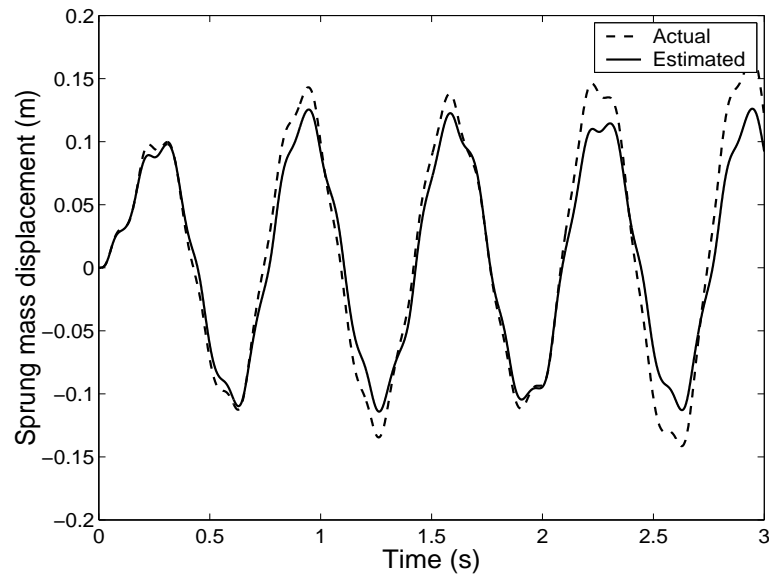


Figure 4.14: Comparison of actual and SMO responses with parametric uncertainties - sinusoidal terrain input

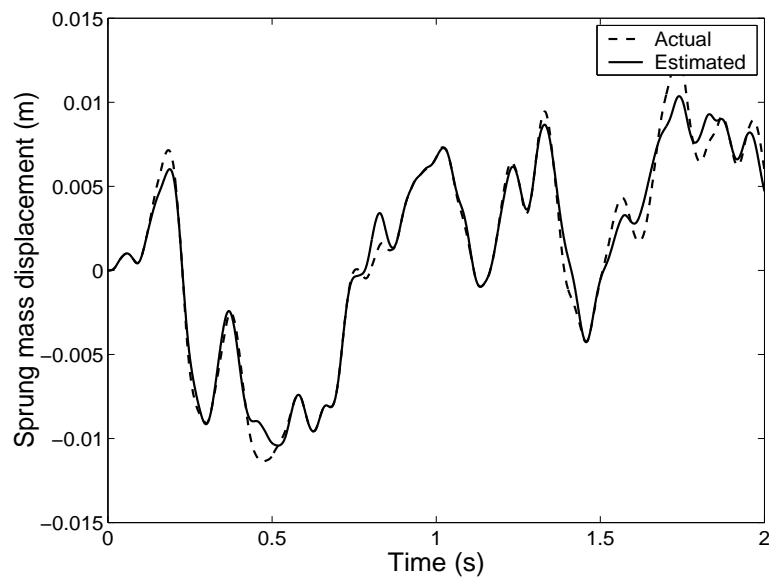


Figure 4.15: Comparison of actual and SMO responses with parametric uncertainties - white noise terrain input

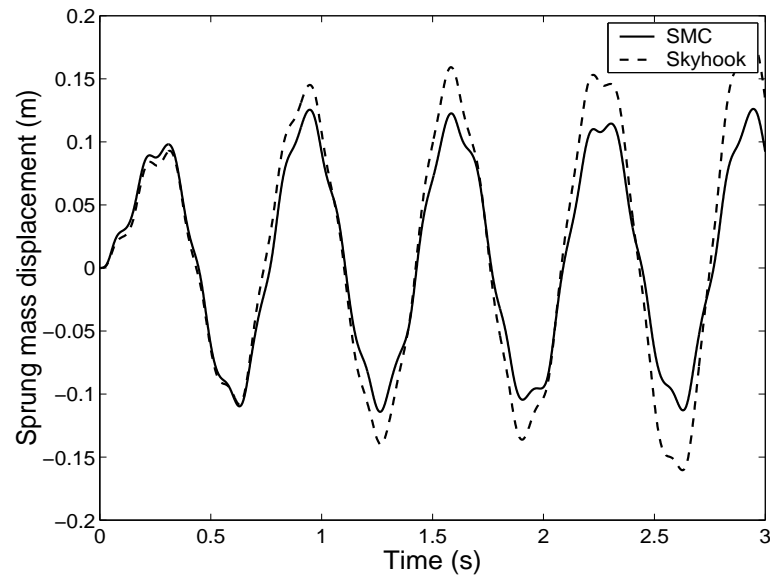


Figure 4.16: Comparison of skyhook reference and SMC responses with parametric uncertainties - sinusoidal terrain input

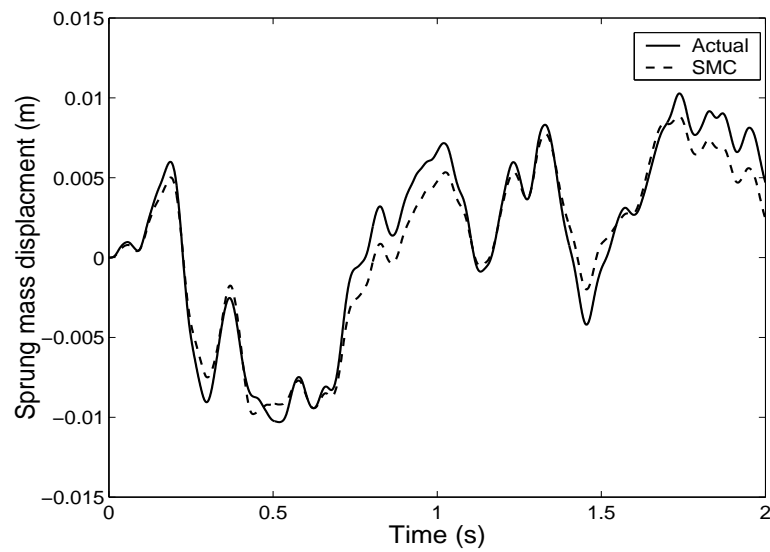


Figure 4.17: Comparison of skyhook reference and SMC responses with parametric uncertainties - white noise terrain input

(without uncertainties). This comparison makes it clear that the SMOC is robust to these uncertainties, as the performance is very similar. The performance to white noise inputs (Figure 4.17) was even better.

4.8 Simulation Set VI: SMC with Unmeasurable Road Inputs

The simulations outlined in previous sections used a model reference control strategy based on the fourth-order, linear and nonlinear skyhook reference models (3.1) and (3.2) shown in Figure 3.2. These reference models require knowledge of the terrain input, which is usually very difficult to measure on a moving vehicle. As explained in Section 3.1.1, an alternative is to use the unsprung mass displacement as the input to a second-order skyhook reference model (3.3) as shown in Figure 3.3. This section outlines the performance implications of using this reduced-order reference model for SMC and SMOC of semiactive vehicle suspensions.

Simulations were conducted using nonlinear versions of the second-order skyhook reference model (3.3) and fourth-order reference model (3.2), and comparing performance for a wide range of road inputs. In each case variable-gain SMC (3.16), assuming full state measurements, was used. For large-amplitude terrain inputs, there were significant differences in the fourth-order and second-order reference model responses, as shown in Figures 4.18 and 4.19. For lower-amplitude road inputs (e.g. white noise and actual road inputs), these differences were less significant. The SMC law was able to track the second-order reference model accurately, as Figures 4.18 and 4.19 show for sinusoidal and impulsive terrain inputs. In every case, however, the fourth-order reference model resulted in superior ride quality.

To evaluate the effect of reference model order on observer performance, simulations were conducted to compare SMOC performance using fourth-order and second-order skyhook reference models. Figures 4.20 and 4.21 show the performance of SMOC for sine wave and “bump” terrain inputs. For the sine wave input (Figure 4.20), the tracking performance of SMOC reduced significantly as compared to SMC (Figure 4.18). However in the process SMOC performance approached that of the fourth-order reference model (3.2). This is also evident by comparing Figures 4.20,4.21 with Figures 4.9,4.10. Hence for large amplitude terrain inputs, the reduction in SMOC tracking performance was acceptable. For low amplitude terrain inputs SMOC tracking performance was comparable to that of SMC.

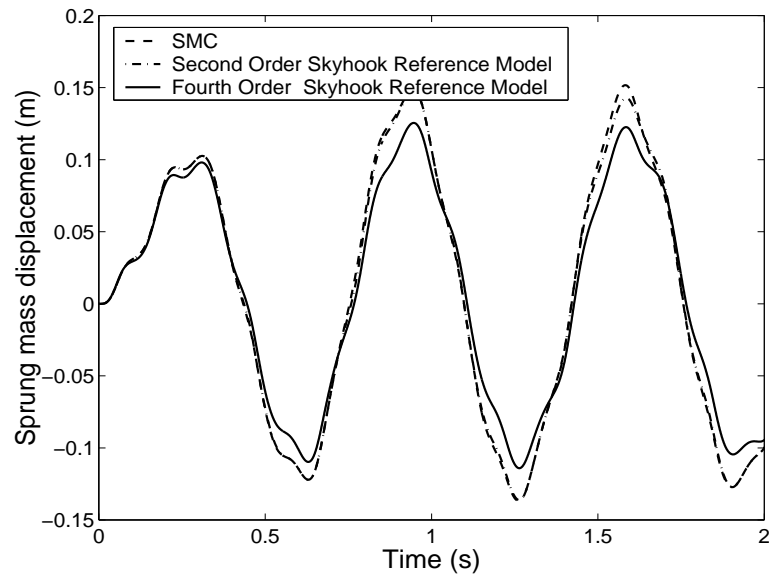


Figure 4.18: Comparison of fourth-order and second-order skyhook reference models - sinusoidal terrain input

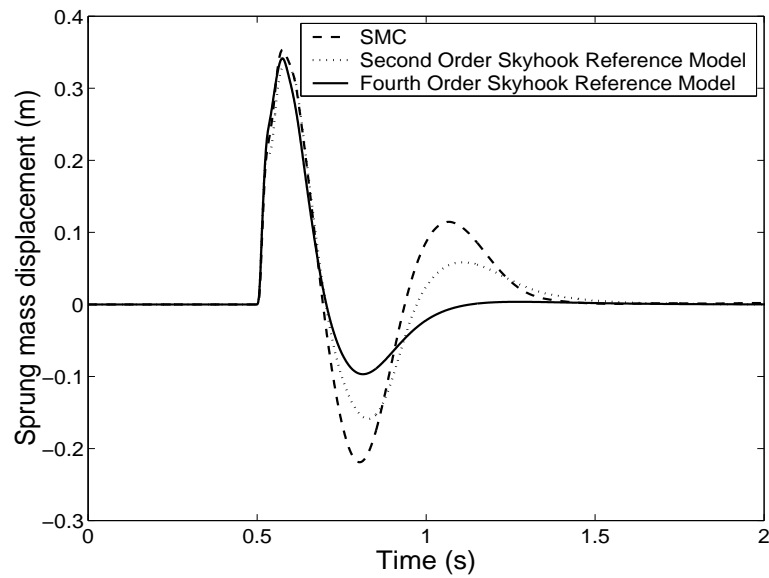


Figure 4.19: Comparison of fourth-order and second-order skyhook reference models - impulse input

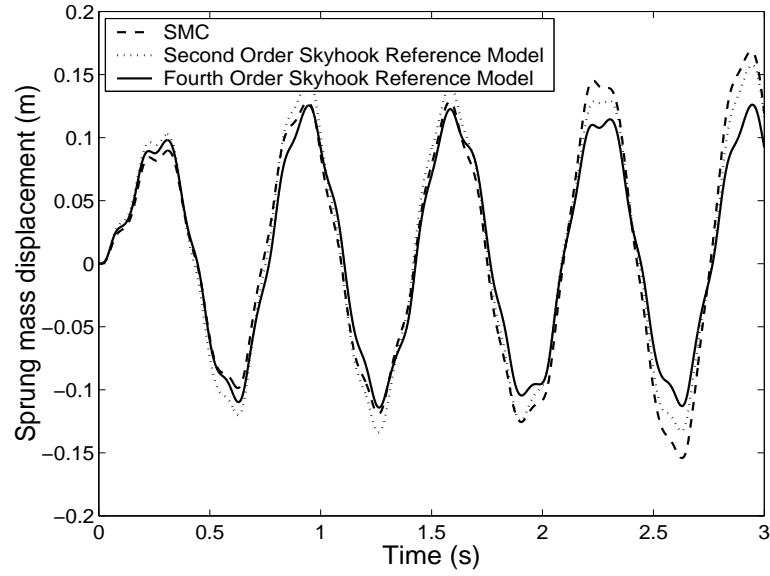


Figure 4.20: SMOC with second-order reference model for sine wave road input

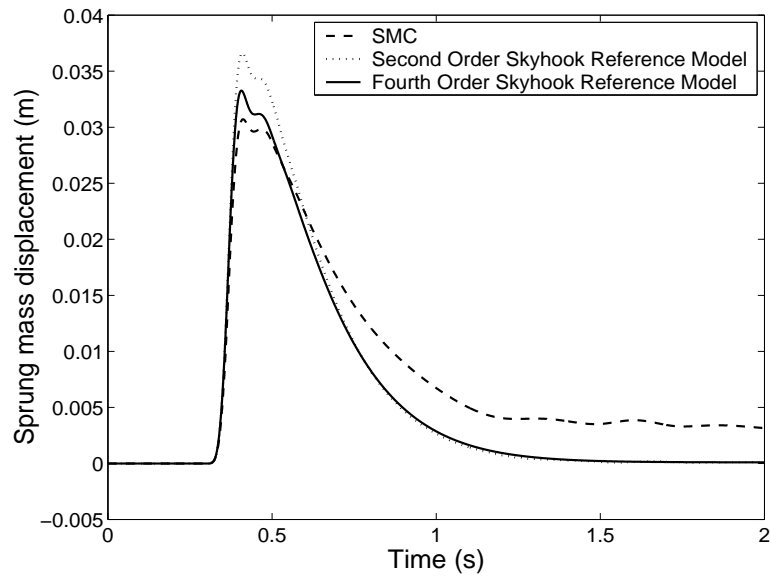


Figure 4.21: SMOC with second-order reference model for "bump" input

In summary, the fourth-order skyhook reference model resulted in better ride quality than the reduced-order reference model (not requiring terrain input knowledge) for all terrain inputs. Model reference SMC and SMOC based on these two models produced similar conclusions. This performance depended on the amplitude and frequency of road inputs, though generally it remained far better than that of conventional passive suspensions.

Chapter 5

Conclusions

Semiactive vehicle suspensions contain nonlinearities and parametric uncertainties that require robust nonlinear control for peak performance. Additionally, the state information required for formulating a control law online is almost never available in practice. While these issues are frequently overlooked in simulations [15,16,19,21], they cannot be overlooked in real-time implementations.

In this research, the performance of sliding mode observation and control for semiactive vehicle suspensions was established through extensive computer simulations. These comprehensive simulations investigated the effects of suspension nonlinearities, parametric uncertainties, and state estimation, and compared performance results with popular alternatives.

Model reference SMC was evaluated using linear and nonlinear skyhook reference models, revealing a significant reduction in ride quality for the nonlinear reference model. This “followability” of this nonlinear reference model was far better, however, making it the preferred reference model for realistic simulations using nonlinear plant models. When compared to popular linear control strategies like LQR, the performance benefits of model reference SMC was apparent. A sliding mode observer was designed and implemented. It performed well for a variety of terrain inputs, even in the presence of parametric uncertainties. The performance and robustness of combined sliding mode observation and control (SMOC) was confirmed through extensive simulations. Finally, the effects of a reduced-order skyhook reference model (not requiring terrain input knowledge) on ride quality and SMC tracking performance was evaluated. Results showed a moderate yet acceptable reduction in performance using the reduced-order reference model.

The results of this research should be directly transferable to actual semiactive vehicle suspension implementations. The effects of realistic nonlinearities, parametric uncertainties, unmeasurable

states and terrain inputs have all been investigated through comprehensive simulations. The results of these simulations reveal the benefits of sliding mode observation and control for improved ride quality.

List of References

- [1] Seung-Jin Heo and Kihong Park, “Performance and design consideration for continuously controlled semi-active suspension systems,” *Int. J. of Vehicle Design*, vol. 23, no. 3, pp. 376–389, 2000.
- [2] R. S. Sharp and S. A. Hassan, “Performance and design considerations for dissipative semi-active suspension systems for automobiles,” *Proc. of the Instn. of Mech. Engrs.*, vol. 201(D2), pp. 149–153, 1987.
- [3] R. S. Sharp and S. A. Hassan, “The relative performance capabilities of passive, active and semiactive car suspension systems,” *Proc. of the Instn. of Mech. Engrs.*, vol. 200(D3), pp. 219–228, 1986.
- [4] G.D. Buckner, K.T. Schuetze, and J. Beno, “Intelligent feedback linearization for active vehicle suspension control,” *to appear, ASME Journal of Dynamic Systems, Measurement and Control*, December 2001.
- [5] G.D. Buckner, K.T. Schuetze, and J. Beno, “Active vehicle suspension control using intelligent feedback linearization,” *Proceedings of the American Controls Conference*, June 2000.
- [6] A. G. Thompson, “Design of active suspensions,” *Proc. of the Instn. of Mech. Engrs.*, vol. 185, no. 36, pp. 553–563, 1970.
- [7] D. A. Crolla, R. H. Pitcher, and J. A. Lines, “Active suspension control for an off-road vehicle,” *Proc. of the Instn. of Mech. Engrs.*, vol. 201(D1), pp. 1–10, 1987.
- [8] Rajesh Ramani and J. K. Hedrick, “Adaptive observers for active automotive suspensions: theory and experiment,” *IEEE Transactions on Control Systems Technology*, vol. 3, no. 1, pp. 41–54, 1995.
- [9] P.G. Wright and D.A. Williams, “The application of active suspension to high performance road vehicles,” *IMEchE conference on Microprocessors in fluid engineering*, 1984.

- [10] S.T. Hung, I. Kanellakopoulos, V. Kokotovic, and P. V. Kokotovic, "Active suspension studies: modeling, identification and analysis," Report AS-88-2, Ford Motor Company, September 1988.
- [11] Scott Memmer, "Suspension iii: active suspension systems," Edmunds Technical Center Articles, <http://www.edmunds.com/ownership/techcenter/articles/43853/article.html>, April 2001.
- [12] D. Z. Wang, S. M. Rohde, and K.P. Oh, "Hydraulic system modeling and simulation in the automotive industry," *Proceedings of the ASME Winter Annual Meeting*, November 1990.
- [13] D. Karnopp, "Theoretical limitations in active suspensions," *Vehicle System Dynamics*, vol. 15, pp. 41–54, 1986.
- [14] Magneshock, "2nd generation magneshock," Carrera Shocks Newsletter, http://www.carrerashocks.com/Newsletter_spring-2001_P1.htm, Spring 2001.
- [15] C. F. Nicolás, J. Landaluze, E. Castrillo, M. Gastón, and R. Rejero, "Application of fuzzy logic control to the design of semiactive suspension systems," *IEEE International Conference on Fuzzy System*, vol. 2, pp. 987–993, 1997.
- [16] D. Hrovat, D. L. Margols, and M. Hubbard, "An approach towards the optimal semi-active suspension," *Transactions of the ASME - Journal of Dynamic Systems Measurement and Control*, vol. 110, pp. 288–296, September 1988.
- [17] J. K. Hedrick, Hong Keum-Shik, and Sohn Hyun-Chul, "Semiactive control of the macpherson suspension system: hardware in the loop simulations," *IEEE Conference on Control Applications*, vol. 1, pp. 982–987, 2000.
- [18] B. Corbett, "Riding the magnetic wave," *Wards Auto World*, p. 49, June 2000.
- [19] Aleksander Hać and Iljoong Youn, "Optimal semi-active suspension with preview based on a quarter car model," *Proceedings of the 1991 American Control Conference*, vol. 1, pp. 433–438, 1991.
- [20] P. J. Th. Venhovens, "The development and implementation of adaptive semi-active suspension control," *Vehicle System Dynamics*, vol. 23, pp. 211–235, 1994.
- [21] Allesandro Guia, Carla Seatzu, and Giampaolo Usai, "Semiactive suspension design with an optimal gain switching target," *Vehicle System Dynamics*, vol. 31, no. 4, pp. 213–232, 1999.
- [22] D. Karnopp, M. J. Crosby, and R. A. Harwood, "Vibration control using semi-active force generators," *Trans. of ASME Journal of Engineering for Industry*, vol. 96, no. 2, pp. 619–626, May 1974.

- [23] Mehdi Ahmadian, “A hybrid semiactive control for secondary suspension applications,” *Proceedings of the ASME, Dynamic Systems and Control Division*, pp. 743–750, 1997.
- [24] Christopher A. Paré, “Experimental evaluation of semiactive magneto-rheological suspensions for passenger vehicles,” M.S. thesis, Mechanical Engineering Department-Virginia Polytechnic Institute and State University, <http://scholar.lib.vt.edu/theses/available/etd-51598-19251/unrestricted/etd.pdf>, May 1998.
- [25] C. Kim and P.I. Ro, “Effect of suspension structure on equivalent suspension parameters,” *Proc. of the Instn. of Mech. Engrs. Part D*, vol. 213, pp. 457–470, 1999.
- [26] A. Stenstrom, C. Asplund, and L. Karlsson, “The nonlinear behavior of a macpherson strut wheel suspension,” *Vehicle System Dynamics*, vol. 23, pp. 85–106, 1994.
- [27] T. J. Gordon and M.C. Best, “Dynamic optimization of nonlinear semiactive suspension controllers,” *International Conference on Control, Part 1*, pp. 332–337, 1994.
- [28] Raseem R. Henry and Ashraf A. Zeid, “A nonlinear sub-optimal, observer-based control for semi-active suspension,” *Transactions of the ASME, Transportation Systems, Dynamic Systems and Control Division*, vol. 44, pp. 181–189, 1992.
- [29] I. Ursu, F. Ursu, T. Sireteanu, and C. W. Stammers, “Artificial intelligence based synthesis of semiactive suspension systems,” *Shock and Vibration Digest*, vol. 32, no. 1, pp. 3–10, January 2000.
- [30] J. C. Smith, Ka C. Cheok, and Huang Ningjian, “Optimal parametric control of a semiactive suspension system using neural networks,” *Proc. of the American Control Conference*, vol. 2, pp. 963–967, 1992.
- [31] Ka. C. Cheok and N. J. Huang, “Lyapunov stability analysis for self-learning neural model with application to semi-active suspension system,” *Proceedings of the IEEE-International Symposium on Intelligent Control*, pp. 326–331, 1989.
- [32] Christopher Edwards and Sarah K. Spurgeon, *Sliding Mode Control: Theory and Applications*, Taylor and Francis, Bristol, PA, 1998.
- [33] C. Kim and P. I. Ro, “A sliding mode controller for vehicle active suspension systems with nonlinearities,” *Proc. of the Instn. Of Mech. Engrs., Part D*, vol. 212, pp. 79–92, 1998.
- [34] Andrew Alleyne and J. K. Hedrick, “Nonlinear adaptive control of active suspensions,” *IEEE Transactions on Control Systems Technology*, vol. 3, no. 1, pp. 94–101, March 1995.

- [35] Makato Yokoyama, J. Karl Hedrick, and Shigehiro Toyama, "A model following sliding mode controller for semi-active suspension systems with mr dampers," *Proceedings of the 2001 American Control Conference*, pp. 2652–2657, June 2001.
- [36] E. K. Bender, "Optimal linear preview control with application to vehicle suspension," *Trans. of ASME Journal of Basic Engineering, part D*, vol. 90, no. 2, pp. 213–221, 1968.
- [37] S.J. Dyke, B.F. Spencer Jr., M.K. Sain, and J.D. Carlson, "Modeling and control of magnetorheological dampers for seismic response reduction," *Smart Materials and Structures*, vol. 5, no. 5, pp. 565–575, October 1996.
- [38] C. Richard, M. R. Cutkosky, and K. Maclean, "Friction identification for haptic display," *Proceedings of the 1999 ASME Dynamic Systems and Control Division*, vol. 67, pp. 324–337, 1999.
- [39] Karl J. Åström, "Control of systems with friction," *Proceedings of the Fourth International Conference on Motion and Vibration Control*, 1998.
- [40] Mark R. Jolly, Jonathan W. Bender, and J. David Carlson, "Properties and applications of commercial magnetorheological fluids," *SPIE 5th Annual Int. Symposium on Smart Structures and Materials, San Diego, CA*, March 1998.
- [41] Shawn P. Kelso, "Experimental characterization of commercially practical magnetorheological fluid damper technology," *Proceedings of SPIE Conference on Smart Structures and Materials, Paper No. 4332-34, Newport Beach, CA*, March 2001.
- [42] Sekhar Raghavan and J. K. Hedrick, "Observer design for a class of nonlinear systems," *Int. Journal of Control*, vol. 59, no. 2, pp. 515–528, 1994.
- [43] J. J. E. Slotine and J. K. Hedrick, "On sliding observers for nonlinear systems," *Journal of Dynamic Systems Measurement and Control*, vol. 109, pp. 245–252, September 1987.
- [44] E. A. Misawa and J. K. Hedrick, "Nonlinear observers-a state of the survey," *Journal of Dynamic Systems Measurement and Control*, vol. 111, pp. 344–352, September 1989.
- [45] A.G. Thompson and C. E. M. Pearce, "Physically realizable feedback controls for a fully active preview suspension applied to a half car model," *Vehicle System Dynamics*, vol. 30, pp. 17–35, 1998.
- [46] Jean Jacques E. Slotine and Weiping Li, *Applied Nonlinear Control*, Prentice Hall, 1991.

- [47] A. Hać, "Adaptive control of vehicle suspension," *Vehicle System Dynamics*, vol. 16, pp. 57–74, 1987.
- [48] William S. Levine, *The Control Handbook*, CRC press, pp. 611-613, 1996.